This is the peer-reviewed, final accepted version for American Mineralogist, published by the Mineralogical Society of America.
The published version is subject to change. Cite as Authors (Year) Title. American Mineralogist, in press.
DOI: https://doi.org/10.2138/am-2020-7381. http://www.minsocam.org/

Revision 1

Precipitation of low-temperature disordered dolomite induced by extracellular polymeric substances of methanogenic Archaea *Methanosarcina barkeri*: Implications for sedimentary dolomite formation

Fangfu Zhang, Huifang Xu*, Evgenya S. Shelobolina, Hiromi Konishi[#], and Eric E. Roden

NASA Astrobiology Institute, Department of Geoscience,

University of Wisconsin - Madison

Madison, Wisconsin 53706

[#] Present address: Department of Geology, Niigata University, 8050 Ikarashi 2-no-cho, Nishi-ku 12 Niigata 950-2181, Japan.

*Corresponding author: Prof. Huifang Xu

Department of Geoscience

University of Wisconsin-Madison

1215 West Dayton Street, A352 Weeks Hall

Madison, Wisconsin 53706

Tel: 1-608-265-5887

Fax: 1-608-262-0693

Email: hfxu@geology.wisc.edu

This is the peer-reviewed, final accepted version for American Mineralogist, published by the Mineralogical Society of America.
The published version is subject to change. Cite as Authors (Year) Title. American Mineralogist, in press.
DOI: https://doi.org/10.2138/am-2020-7381. http://www.minsocam.org/

ABSTRACT

A correlation between methanogenesis and dolomite formation has been reported; however, the mechanism underlying of this association is not fully understood. In this study, we conducted forced carbonate precipitation experiments at room temperature in calcite-seeded Ca/Mg carbonate solutions containing either purified non-living biomass or bound extracellular polymeric substances (EPS) of the methanogen *Methanosarcina barkeri.* Purified non-living biomass and bound EPS was used so as to avoid the possible influence of the complex components of the growing microbial culture on carbonate crystallization. Our results demonstrated that non-living biomass of *M. Barkeri* can enhance the Mg incorporation into calcitic structure and induce the crystallization of disordered dolomite. In the presence of ~113 mg/L of non-living biomass, disordered dolomite with ~41 and 45 mol% of $MgCO_3$ was precipitated in solutions with initial Mg:Ca ratios of 5:1 and 8:1, respectively. A systematic increase in the $MgCO_3$ contents of the precipitated Ca-Mg carbonates was also observed with the increased non-living biomass concentration. Bound EPS was shown to be the component of non-living biomass that catalyzed the precipitation of disordered dolomite. At only ~25 mg L^{-1} of bound EPS, disordered dolomite with ~47 and 48 mol% of $MgCO_3$ was precipitated in solutions with initial Mg:Ca ratios of 5:1 and 8:1, respectively. We propose that adsorption of bound EPS to growing carbonate surfaces through hydrogen bonding is the key to catalyzing disordered dolomite crystallization, and that this mechanism is also applicable to natural EPS-induced dolomite formation. This study provides significant insight into the formation mechanism of microbial-induced dolomite with heavy $\delta^{13}C$ values.

Key words: sedimentary dolomite, methanogen, EPS, catalysis, microbial-induced dolomite, heavy $\delta^{13}C$ value

INTRODUCTION

Although abundant in ancient rocks, dolomite is uncommon in modern sedimentary environments. Present-day low-temperature dolomite formation is usually observed in association with marine and other saline environments (Jones 1961; Zenger et al. 1980; Machel and Mountjoy 1986; Hardie 1987; Mazzullo 2000; Warren 2000). Freshwater dolomite has also been documented but its occurrence is rare (El-Sayed et al. 1991; Colson and Cojan 1996; Capo et al. 2000; Whipkey et al. 2002; Roberts et al. 2004; Kenward et al. 2009). The rarity of modern dolomite is largely consistent with the notorious difficulty in reproducing dolomite crystallization under ambient conditions (Lippmann 1973; Oomori and Kitano 1987; Land 1998; Higgins and Hu 2005), contributing to the long-existing controversy over the formation mechanism of sedimentary dolomite, i.e. the "dolomite problem" (Zenger et al. 1980; Machel and Mountjoy 1986; Hardie 1987; Burns et al. 2000; Mazzullo 2000; Warren 2000).

While there is no simple abiotic recipe for dolomite precipitation, recent studies suggest that microbes are paramount to overcoming kinetic barriers to dolomite crystallization. A number of metabolic pathways have been implicated in catalyzing dolomite precipitation, including both bacterial sulfate reduction (BSR) and methanogenesis (Baker and Kastner 1981; Baker and Burns 1985; Hardie 1987; Compton 1988; Vasconcelos and McKenzie 1997; Wright 1999; Burdige et al. 2000; Mazzullo 2000; Warren 2000; Van Lith et al. 2003b; Roberts et al. 2004; Kenward et al. 2009; Deng et al. 2010). Many carbonate precipitation studies have been performed exploring the poorly constrained role of sulfate-reducing bacteria (SRB) in promoting dolomite precipitation (Vasconcelos et al. 1995; Nielsen and Jahn 1999; Warthmann et al. 2000; Van Lith et al. 2003b; Wright and Wacey 2005; Kenward et al. 2009; Deng et al. 2010; Krause et al.; Zhang et al. 2012a; Xu et al. 2013; Zhang et al. 2013). For example, Zhang *et al.* (2012a)

demonstrated the catalytic role of dissolved sulfide, one of the major products of BSR, in dolomite precipitation. However, fewer studies have been devoted to methanogens, although there may exist some physiochemical rules which are common to dolomite induced by SRB and methanogens. Roberts *et al.* (2004) and Kenward *et al.* (2009) conducted Ca-Mg carbonate precipitation experiments in natural environment and culture media respectively, with the involvement of methanogens and showed dolomite precipitation in natural environment. Recent molecular dynamics modeling also proves that polysaccharides (main components in EPS) can lower the dehydration energy barrier (Shen et al. 2015).

In natural environments, the vast majorities of microorganisms live and grow in aggregated forms such as biofilms and flocs. The common feature of all these phenomena is that microorganisms are embedded in an EPS matrix. The production of EPS matrix has been shown to occur both in prokaryotic and eukaryotic microorganisms (Nielsen and Jahn 1999; Wingender et al. 1999). EPS is composed of organic macromolecules including polysaccharides, proteins, nucleic acids, (phospho)lipids, and other polymeric compounds. Their composition may be controlled by different processes, such as active secretion, shedding of cell surface material, cell lysis, and adsorption from the environment (Wingender et al. 1999). Reported functions of EPS matrix include mediating cell adhesion to surfaces and metabolic interactions between cells and minerals, templating mineral crystallization, aggregation of cells in flocs and biofilms, stabilization of the biofilm structure, formation of a protective barrier that provides resistance to biocides, protection from UV radiation, toxic metals, the toxicity of mineral surfaces or other harmful effects, retention of water, and sorption of exogenous organic compounds for the accumulation of nutrients from the environment (Geesey et al. 1988; Costerton et al. 1995; Laspidou and Rittmann 2002; Chan et al. 2004; Harrison et al. 2007; Xu et al. 2012). EPS can

also influence carbonate precipitation in multiple ways (Reid et al. 2000; Dupraz et al. 2009). Negatively-charged acidic groups within the EPS matrix can effectively bind metal cations (Li et al. 2001; Perry et al. 2005; Ortega-Morales et al. 2006; Braissant et al. 2007), which can therefore remove free Ca^{2+} ions from solution, inhibiting carbonate precipitation when limited Ca^{2+} ions are available from the proximal surrounding environment (Kawaguchi and Decho 2002; Dupraz et al. 2004; Dupraz and Visscher 2005; Gautret and Trichet 2005). Subsequently, the degradation of the labile fraction of EPS, abiotically or biotically, can liberate Ca^{2+} bound to the polymer to promote carbonate precipitation (Dupraz and Visscher 2005; Dupraz et al. 2009). EPS can also provide nucleation sites for carbonates (Fortin et al. 1997; Nielsen and Jahn 1999; Dupraz and Visscher 2005; Bontognali et al. 2008; Dupraz et al. 2009; Bontognali et al. 2010; Paulo and Dittrich 2013).

In laboratory pure cultures, however, EPS matrix is not essential structure of microorganisms, since loss of EPS matrix does not impair growth and viability of the cells as it does in naturals systems (Nielsen and Jahn 1999; Wingender et al. 1999). Also, the definition of EPS in pure cultures is often slightly different from that used in natural systems. EPS in pure cultures is often divided into two categories: bound and soluble EPS (Hsieh et al. 1994; Nielsen et al. 1997; Nielsen and Jahn 1999; Laspidou and Rittmann 2002). Bound EPS includes sheaths, capsular polymers, condensed gel, loosely bound polymers, and attached organic materials. Soluble EPS includes soluble macromolecules, colloids, and slimes. Bound EPS is associated with the cell surface and is presumably crucial for biofilm formation, whereas soluble EPS is loosely associated with the cells and predominantly generated by sloughing off from bound EPS (Xu et al. 2012).

This is the peer-reviewed, final accepted version for American Mineralogist, published by the Mineralogical Society of America.
The published version is subject to change. Cite as Authors (Year) Title. American Mineralogist, in press.
DOI: https://doi.org/10.2138/am-2020-7381. http://www.minsocam.org/

In previous laboratory dolomite precipitation experiments within live culture of SRB and methanogen, the involvement of bound EPS has been shown in promoting dolomite nucleation and growth (Van Lith et al. 2003b, a; Roberts et al. 2004; Bontognali et al. 2008; Kenward et al. 2009; Bontognali et al. 2014). However, within live cultures, a definitive elucidation of the effect of bound EPS on dolomite precipitation can be hard to reach, since microbes, microbial metabolic products, and the complex ingredients of typical culture medium may all affect carbonate precipitation. For example, phosphate in SRB culture media can lead to the precipitation of Ca/Mg-phosphate minerals. It also has a pronounced impact on carbonate precipitation and can potentially obscure or alter more subtle effects on mineral precipitation, which might lead to misinterpretation of culture studies meant to simulate natural systems (Gallagher et al. 2013). Some claimed dolomite precipitates are actually aragonite (Wright & Wacey (2005), see their Figure 14A) and Ca-Mg-phosphates. Recently studies show that addition of low dipole moment substances, such as H_2S, carboxylic acid, and methane, can change the behavior of the solution, disrupt surface Mg^{2+}-water complex, and promote Mg incorporation into Ca-Mg-carbonates (Xu 2010; Zhang et al. 2010). Substrates like (001) surfaces of clay minerals and hematite can promote heterogeneous nucleation of calcite and high magnesian calcite, and inhibit aragonite formation due to their pseudo-hexagonal (001) surfaces (Xu et al. 2018). Low temperature abiotic synthesis with addition of smectite show precipitation of disordered dolomite (Liu et al. 2019)

In this study, we characterized the effect of bound EPS from the methanogen *Methanosarcina barkeri* on Ca-Mg carbonate precipitation. *M. barkeri* is a anaerobic methanogenic archaea commonly isolated from mud samples in lakes and bogs and sewage samples (Stadtman and Barker 1951; Balch et al. 1979; Hippe et al. 1979; Bock et al. 1994;

Maeder et al. 2006). *M. barkeri* is metabolically versatile and can utilize a variety of methanogenic substrates including H_2, CO_2, methanol, methylamines, and acetate. This species can also adapt to one of the widest ranges of habitats for an individual methanogenic species, from freshwater to high salinity water with three times the solute concentration in seawater. Laboratory culture studies showed that it exhibits a dichotomous morphology, growing in freshwater as large multicellular aggregates embedded in an EPS matrix, or in high extracellular solute concentrations as individual cells without EPS (Stadtman and Barker 1951; Sowers et al. 1993; Anderson et al. 2012). In this study, we cultured *M. barkeri* in freshwater medium so that we could (1) collect sufficient amount of bound EPS for carbonate precipitation experiments and (2) gain a broader understanding of the potential role of methanogens in freshwater dolomite formation. To the best of our knowledge, no evidence has been shown to demonstrate the presence of *M. barkeri* in natural dolomite formation. However, this does not necessarily suggest that *M. barkeri* was irrelevant to dolomite formation. Instead, a study with *M. barkeri* may provide a chance to evaluate if dolomite formation is tied to certain microorganism species and explore the geochemical and thermodynamic/kinetic "rules" which are common to all dolomite (Pursher et al. 1994).

Instead of live cultures, we used purified bound EPS, non-living biomass and dead cell pellets (DCP) after bound EPS extraction for forced carbonate precipitation experiments at room temperature in calcite-seeded solutions. This procedure avoided the possible influence of complex components of typical cultures, which therefore makes it possible to clearly assess the contribution of bound EPS/non-living biomass/DCP to Ca-Mg carbonate precipitation. Our data demonstrated that bound EPS of *M. barkeri* can promote the incorporation of Mg into precipitating Ca-Mg carbonates and induce disordered dolomite precipitation. We propose a

plausible mechanism by which surface adsorbed bound EPS catalyzes Mg incorporation into anhydrous Ca-Mg-carbonate. We also discussed the implications of this study to the long-lasting "dolomite problem".

This is the peer-reviewed, final accepted version for American Mineralogist, published by the Mineralogical Society of America.
The published version is subject to change. Cite as Authors (Year) Title. American Mineralogist, in press.
DOI: https://doi.org/10.2138/am-2020-7381. http://www.minsocam.org/

MATERIALS AND METHODS

Microorganisms and culture medium

The culture of *M. barkeri* strain MS (neotype strain) (DSM 800) was obtained from the German Collection of Microorganisms (DSMZ). *M. barkeri* was cultivated in a near neutral pH medium (pH 6.5-6.8) with the following composition (per liter): K_2HPO_4 0.348 g, KH_2PO_4 0.227 g, NH_4Cl 0.5 g, $MgSO_4 \cdot 7H_2O$ 0.5 g, $CaCl_2 \cdot 2H_2O$ 0.25 g, NaCl 2.25 g, $FeSO_4 \cdot 7H_2O$ 0.002 g, vitamin solution (Wolin et al. 1963) 10 ml, trace element solution (Whitman et al. 1982; Bock et al. 1994) 1 ml, yeast extract (Difco) 2 g, $NaHCO_3$ 0.85 g, methanol 10 ml, cysteine-$HCl \cdot H_2O$ 0.3 g, and $Na_2S \cdot 9H_2O$ 0.3 g. The medium was prepared anoxically under a N_2:CO_2 (80:20 v/v) atmosphere. Methanol (50% v/v), $NaHCO_3$, $Na_2S \cdot 9H_2O$, $MgSO_4 \cdot 7H_2O$, and $CaCl_2 \cdot 2H_2O$ were added separately from sterile stock solutions after the medium was autoclaved. The stock solution of $NaHCO_3$ was prepared under a N_2:CO_2 (80:20 v/v) atmosphere, whereas those of methanol, $Na_2S \cdot 9H_2O$, $MgSO_4 \cdot 7H_2O$, and $CaCl_2 \cdot 2H_2O$ were under 100% N_2.

Biomass collection

Biomass from *M. barkeri* was collected in the early stationary growth phase. The pH of the culture when collecting biomass was ~5.2. No precipitates were observed in either cell-free medium or live culture. Cultures were first centrifuged at 15,000 rpm for 30 min with a Beckman-Coulter Avanti® J-E centrifuge. The supernatant was discarded and the biomass was then washed with a N_2-sparged washing buffer containing all the inorganic ingredients in the medium but not the organic ones and Na_2S. The purpose of such wash was to remove the possible residue organics from the medium and other soluble microbial metabolites. The washing buffer carried an ionic strength and composition close to that of the medium; otherwise some bound EPS components might desorb and thus be washed away from the EPS matrix (Nielsen

and Jahn 1999). The washing buffer with the biomass was centrifuged at 15,000 rpm for 20 min and the supernatant was discarded. After that, ~40 ml of washing buffer was added to the washed biomass (~10-26 mg), which was then dialyzed against distilled de-ionized (DI) water for 24 h and collected for carbonate precipitation experiments. The biomass was non-metabolizing after dialysis since it was exposed to air during dialysis. To measure the dry weight of biomass in solution, a portion of the biomass solution was freeze dried at -50°C for 48 h.

Extraction and quantification of bound EPS

The bound EPS of *M. barkeri* was extracted in the stationary growth phase. Biomass of *M. barkeri* was concentrated and washed following the same procedure above. Next, washing buffer was added to the washed biomass to obtain a biomass concentration of 1.0 mg mL^{-1} and bound EPS was extracted from this biomass solution following a previously established procedure developed for methanogenic sludges that utilizes formaldehyde and NaOH (Liu and Fang 2002). It has been shown that this procedure can prevent the extracted bound EPS from the contamination by intracellular substances (Nielsen and Jahn 1999; Liu and Fang 2002). The detailed procedure is shown in **Fig. 1**. To obtain the concentration of bound EPS in solution, a portion of dialyzed bound EPS solution was freeze dried at -50°C for 48 h for measuring the dry weight. The residue DCP was also collected by adding ~40 ml of washing buffer to the residue pellets and dialysis against DI water for 24 h.

The total carbohydrate content of bound EPS was measured using a modified phenol-sulfuric acid method with glucose standards (Dubois et al. 1956). Polysaccharides (or other monomeric sugars in EPS) were first hydrolyzed to individual monosaccharides with H_2SO_4 (Pakulski and Benner 1992). To do this 1 mg of dry EPS was added into 1 mL of 12 M H_2SO_4 at

room temperature for 2 h. Then 9 mL DI water was added to the slurry. Samples were briefly (3-5 s) ultrasonicated to promote the dissolution of the residue. A 5 mL aliquot of the solution was pipetted into a 50 mL serum vial, crimp-sealed with Teflon liners and hydrolyzed at 100°C for 3 h. Then 1 mL aliquot was added in a test tube followed by 1 mL of phenol solution (5%) and 5 mL of 98% sulfuric acid. The tube was shaken well on a shaker. After 10 min, it was placed in a water bath at 30°C for 20 min. The mixture was cooled and measured for absorbance at 490 nm using an UV-Vis spectrophotometer (UV-mini 1240, Shimadzu Corp, Kyoto, Japan). The final results were normalized by the dry weight of bound EPS. Bound EPS collected from three batches of the culture was analyzed and duplicate aliquots were analyzed for each bound EPS sample. All experimental glassware used in these analyses was acid washed, rinsed with DI water, and combusted at 550°C for 6 h to prevent the possible organic contamination.

Sugar monomer analyses were performed to investigate the monosaccharide composition of the bound EPS of *M. barkeri*. This monomer composition of intact EPS was measured through glycosyl analyses using gas chromatography combined mass spectrometry (GC/MS) of the per-O-trimethylsilyl (TMS) derivatives of the monosaccharide methyl glycosides produced from the sample by acidic methanolysis. 400 μg of the sample was used for the analysis. 20 μg of inositol was added to the sample as an internal standard. Methyl glycosides were then prepared from the dry sample by methanolysis in 1 M HCl in methanol at 80°C (18 h), followed by re-N-acetylation with pyridine and acetic anhydride in methanol (for detection of amino sugars). The sample was then per-O-trimethylsilylated by treatment with Tri-Sil (Pierce) at 80°C (0.5 h). These procedures were carried out as previously described (York et al. 1986; Merkle and Poppe 1994). GC/MS analysis of the TMS methyl glycosides was performed on an Agilent 6890N GC

interfaced to a 5975B MSD, using an Agilent DB-1 fused silica capillary column (30 m × 0.25 mm ID).

Forced carbonate precipitation experiments with non-metabolizing biomass, bound EPS and DCP

All carbonate precipitation experiments were carried out at room temperature (22 ºC) and at least two duplicates were performed. All the glassware used in the synthesis was acid-washed, rinsed with DI water and baked at 550°C for 6 h to prevent the possible organic contamination. Solutions containing non-metabolizing *M. barkeri* biomass/bound EPS/DCP were diluted with DI water to obtain a range of bulk concentrations **(see Table 1)**. Reagent grade $CaCl_2 \cdot 2H_2O$ and $MgCl_2 \cdot 6H_2O$ powders were then added to the solutions. The concentration of $CaCl_2$ was fixed at 5 mM, whereas different concentrations of $MgCl_2$ were used (15 20 25 and 40 mM). The calcite seeds were synthesized by mixing equal volumes of 500 mM $CaCl_2$ and 500 mM $NaHCO_3$. X-ray diffraction (XRD) analysis showed that calcite was the only phase in the synthetic seeds. Scanning electron microscopy (SEM) examinations showed that the size of synthetic seeds was usually several microns. The specific surface area of the seed crystals, as determined by multi-point N_2 BET method (Brunauer et al. 1938), was 0.2 $m^2 g^{-1}$. Synthetic calcite crystals with size range of 10 ~ 20 micrometers (0.2 g/L) were used as seeds for heterogeneous nucleation. Previous studies showed that presence of calcite seed can promote the incorporation of Mg into calcitic structure and inhibit aragonite precipitation (Berner 1975; Zhang et al. 2012a). Experimental solutions containing biomass/bound EPS/DCP were ultrasonicated for 10 min to suspend synthetic seeds and then left still for overnight so that solutions can be equilibrated with atmospheric CO_2 and calcite seeds. After that, the pH of experimental solutions was measured as

This is the peer-reviewed, final accepted version for American Mineralogist, published by the Mineralogical Society of America.
The published version is subject to change. Cite as Authors (Year) Title. American Mineralogist, in press.
DOI: https://doi.org/10.2138/am-2020-7381. http://www.minsocam.org/

the initial pH **(Table 1)**. A geochemical program (PHREEQC) was utilized to calculate the starting chemical compositions of the control solutions (Parkhurst and Appelo 1999). The starting pH of the control solutions and PHREEQC calculations suggested that approximately 0.03-0.04 g/L out of the 0.2 g/L calcite seeds were dissolved and the control solutions were equilibrated with atmospheric CO_2.

Forced carbonate precipitation experiments were conducted with a NH_4HCO_3 drift-free method (Lian et al. 2006). Crystallization reactions took place in a desiccator (dimensions 36 × 36 × 41 cm). A number of Petri dishes containing experimental solutions were placed in the desiccator, along with some NH_4HCO_3 powders (5 g for a total experimental solution volume of 500 mL) contained in separate Petri dishes. NH_3 and CO_2 produced from the decomposition of NH_4HCO_3 diffused into experimental solutions where carbonate precipitation occurred. After 14 days, precipitates were collected by filtering solutions through a 0.22 μm membrane, rinsed with DI water for several times, and air-dried. The concentrations of Ca^{2+} and Mg^{2+} in solutions were also measured with inductively coupled plasma optical emission spectroscopy (ICP-OES, Varian Vista-MPX, Australia) both before and after experiments at least in duplicates for each experimental condition. Parallel control experiments were carried out with organic-free solutions. Detailed chemical conditions in carbonate precipitation experiments are listed in **Table 1**.

PHREEQC was also used to calculate the saturation index (SI) of control solutions with respect to disordered dolomite with ideal dolomite composition (50 mol% of $MgCO_3$). SI is defined as SI = Log(IAP/*K*sp), whereas the IAP is the ion activity product of the dissolved mineral constituents and *K*sp is the equilibrium constant, that is $10^{-16.52}$ for disordered dolomite (Carpenter 1980). We did not calculate SI for experimental solutions containing non-metabolizing biomass/EPS/DCP since they can bind metal cations as discussed above and we did

not find data on their binding capacity. However, the SI of control solutions should be higher than that of experimental solutions due to the presence of more available metal cations.

XRD, SEM, transmission electron microscopy (TEM) and selected-area electron diffraction (SAED) examinations

XRD analyses were carried out using a Rigaku Rapid II X-ray diffraction system (Mo $K\alpha$ radiation). Samples were contained in thin-wall glass capillaries. Diffraction data were collected on a 2-D image-plate detector. The two-dimensional images were then integrated to produce conventional 2θ vs. intensity patterns using Rigaku's 2DP software.

SEM samples were prepared by dispersing powders on carbon tapes and lightly carbon coated (50-100 Å coating). SEM observations were performed using a LEO 1530 SEM equipped with energy-dispersive spectroscopy (EDS) capabilities to determine the solid-phase composition.

TEM and SAED measurements were done with an aberration-corrected FEG-(S)TEM (Titan 80-200) which is capable of sub-Å-resolution structural and chemical imaging. Several milligrams of sample were crushed between two glass slides with a few drops of ethanol. A drop of the resulting suspension was placed on a holey carbon film supported by a TEM Cu grid and air-dried.

Bulk average $MgCO_3$ content of synthetic Ca-Mg carbonates was measured based on the empirical curve correlating the shift of calcite (104) peak toward dolomite and $MgCO_3$ contents (Zhang et al. 2010). TEM-based X-ray EDS was also used to measure $MgCO_3$ contents of typical disordered dolomite samples (for method details, see Zhang *et al.* (2010)).

Terminology of Ca-Mg carbonates

Ideal dolomite ($CaMg(CO_3)_2$, space group: $R\bar{3}$) has a crystal lattice consisting of alternating layers of Ca and Mg, separated by layers of CO_3, where Ca and Mg are present in equal proportions. However, very few, if any, sedimentary dolomites are truly stoichiometric $CaMg(CO_3)_2$ and are better represented as: $Ca_{(1+x)}Mg_{(1-x)}(CO_3)_2$. Most ancient dolomites are calcium-rich (Warren 2000).

Mg^{2+} incorporation into calcitic structure results in the formation of various phases, including: low-Mg calcite (LMC, space group: $R\bar{3}c$) with less than 4 mol% of $MgCO_3$, high Mg-calcite (HMC, space group: $R\bar{3}c$) with more than 4 mol% and less than 36 mol% of $MgCO_3$ according to the proposed solvus between calcite and dolomite (Anovitz and Essene 1987), disordered dolomite (with more than 36 mol% of $MgCO_3$ and typically Ca-rich with disordered cations, i.e., instead of occurring in alternating cation layers, Ca^{2+} and Mg^{2+} ions are randomly distributed; therefore, it has the same space group as calcite: $R\bar{3}c$), and dolomite (space group: $R\bar{3}$) (Zhang et al. 2012a). Proto-dolomite is a poorly ordered dolomite, and generally Ca-rich (Fang and Xu 2018).

This is the peer-reviewed, final accepted version for American Mineralogist, published by the Mineralogical Society of America.
The published version is subject to change. Cite as Authors (Year) Title. American Mineralogist, in press.
DOI: https://doi.org/10.2138/am-2020-7381. http://www.minsocam.org/

RESULTS

Saturation state of experimental solutions

After NH_4HCO_3 powder and the petri dishes containing solutions were put into the sealed dessicator, the decomposition of NH_4HCO_3 started shortly and carbonate precipitation was observed in 6-8 hours as indicated by the visual cloudiness in the solution. NH_4HCO_3 powders were totally decomposed in ~12 hours. The pH measured one day after experiments started was fairly close to final pH measured after 14 days **(Table 1)**. We used PHREEQC to calculate the SI of control solutions with respect to disordered dolomite (SI_{dd}). However, we encountered several problems during calculation, which prevented us from obtaining specific numbers for SI_{dd}. First, based on calculation, all the NH_3 and ~ 90% of CO_2 produced by NH_4HCO_3 decomposition should be dissolved into the solution, which would produce a final pH of ~8.2. This calculation is not supported by our observations that (1) the final pH was ~9.2-9.3 in all controls; (2) there was still a strong smell of NH_3 gas after 14 days. Second, carbonate precipitation started before all the NH_4HCO_3 was decomposed. To overcome this, we first used the final Ca^{2+} and Mg^{2+} concentrations in control solutions after precipitation and a trial-and-error procedure to adjust the dissolved NH_3 and CO_2 concentration to match the final pH. We found that calculated pH will best fit the final measured pH if half of the NH_3 (31 mmol) and one quarter of CO_2 (15.8 mmol) produced by the decomposition of 5 g NH_4HCO_3 are dissolved into 500 mL solution. A SI_{dd} calculated under these conditions was noted as the final SI_{dd} or the lowest SI_{dd}. Then since (1) the pH of the solution was buffered by the dissolved NH_3 and CO_2 and (2) the pH measured one day after experiments started was fairly close to final pH, we assumed that when massive carbonate precipitation started, the amounts of dissolved NH_3 and CO_2 were also 31 mmol and 15.8 mmol for 500 mL solution, respectively. We used such numbers along with the measured initial Ca^{2+}

and Mg^{2+} concentrations to calculate another SI_{dd}, noted as the initial SI_{dd} or the highest SI_{dd}. Calculated SI_{dd} is listed in **Table 1**. We want to emphasize that the SI_{dd} of control solutions should be higher than that of experimental solutions containing non-metabolizing biomass or bound EPS due to the presence of more available metal cations.

Ca-Mg carbonates induced by non-metabolizing biomass, bound EPS, and DCP

XRD analyses of precipitated carbonates showed that non-metabolizing biomass can promote Mg incorporation and Ca-Mg carbonate precipitation, especially in solutions with high initial Mg:Ca ratios. For example, when the initial Mg:Ca ratio in solution was 3:1 or 4:1, the $MgCO_3$ contents of HMC precipitated in experimental solutions containing ~113 mg L^{-1} of non-metabolizing biomass were not significantly higher than the carbonate precipitated in control solutions **(Fig. 2a, b; Fig. S1a, b)**. However, the catalytic effect of non-metabolizing biomass became much more obvious with increased initial Mg:Ca ratios. Ca-Mg carbonates with ~41 and ~45 mol% of $MgCO_3$ was precipitated in experimental solutions with an initial Mg:Ca ratio of 5:1 and 8:1, respectively **(Fig. 2c, d; Table 1)**, while control solutions produced HMC with only ~12 and ~18 mol% of $MgCO_3$, respectively **(Fig. S1c, d)**. In addition, the non-metabolizing biomass also inhibited the precipitation of aragonite **(compare Fig. 2 and S1)** which is generally believed to compete with the crystallization of Ca-Mg carbonates (Lippmann 1973; Berner 1975).

The catalytic effect of non-metabolizing biomass was also supported by experiments with different non-metabolizing biomass concentrations. The $MgCO_3$ contents in the synthetic Ca-Mg carbonates increased with non-metabolizing biomass concentration **(Fig. 3, 4a, S2; Table 1)**. Increased non-metabolizing biomass concentration also reduced the amount of aragonite in the precipitates **(compare Fig. 2 and 3)**. With the highest concentration of biomass (~161 mg L^{-1}),

monohydrocalcite ($CaCO_3 \cdot H_2O$) also appeared **(Fig. 3)**. This trend is consistent with previous studies on Ca-Mg carbonate precipitation in solutions with dissolved sulfide as catalyst, which showed that while dissolved sulfide can promote dolomite precipitation, over-dosed dissolved sulfide triggered monohydrocalcite crystallization (Zhang et al. 2012a).

Monohydrocalcite was the only crystalline phase identified in the carbonates precipitated in experimental solutions with 161mg L^{-1} of non-metabolizing biomass and an initial Mg:Ca ratio of 8:1 **(Fig. 3d)**. We suggest that an amorphous Ca-Mg carbonate phase was precipitated in addition to monohydrocalcite as indicated by the Mg removed from the solution **(Table 1)**. The high concentrations of Ca^{2+} left in the solution may also reflect the formation of amorphous Ca-Mg carbonates since the amorphous Ca-Mg carbonates have higher solubility than the crystalline counterparts.

Precipitation experiments were carried out to assess the effect of bound EPS excreted by *M. barkeri* on carbonate precipitation. Approximately 25 mg bound EPS could be extracted from ~113 mg biomass. Our results clearly demonstrated the catalytic role of bound EPS in Ca-Mg carbonate precipitation. The $MgCO_3$ contents of Ca-Mg carbonates induced by bound EPS were generally higher than those by non-metabolizing biomass at same initial Mg:Ca ratio **(Fig. 4b, 5; Table 1)**. Ca-Mg carbonates with ~47 and ~48 mol% of $MgCO_3$ was precipitated in experimental solutions with bound and an initial Mg:Ca ratio of 5:1 and 8:1, respectively **(Fig. 5c, d; Table 1)**.

DCP slightly enhanced Mg incorporation compared to control experiments **(Fig. 6; Table 1)**. However, the $MgCO_3$ contents of carbonates precipitated in DCP-bearing solutions were generally much lower than those induced by bound EPS, except in experiments with an initial Mg:Ca ratio of 8:1 which precipitated both HMC and Ca-Mg carbonates close to dolomite **(Fig.**

This is the peer-reviewed, final accepted version for American Mineralogist, published by the Mineralogical Society of America.
The published version is subject to change. Cite as Authors (Year) Title. American Mineralogist, in press.
DOI: https://doi.org/10.2138/am-2020-7381. http://www.minsocam.org/

384 **6d)**. Precipitates in DCP-bearing solutions also contained more aragonite than those induced by
385 bound EPS. These data indicate that bound EPS was the active component in the non-
386 metabolizing biomass that promoted the precipitation of Ca-Mg carbonates close to dolomite
387 composition.

388 High-resolution SEM and TEM observations showed Ca-Mg carbonates close to
389 dolomite composition occurred as nano-crystals (~10-20 nm) overgrowing euhedral calcite seeds
390 **(Fig. 7, 8a, b)**. On some calcite seeds, the overgrowing carbonates were not massive, which
391 therefore preserved the overall rhombohedral shape of calcite seed **(Fig. 7a)**. However, in the
392 case of massive overgrowth, nano-crystals of Ca-Mg carbonate close to dolomite composition
393 enclosed calcite seeds and formed clusters with different shapes and sizes **(Fig. 7c)**. SAED
394 patterns showed that nano-crystals of Ca-Mg carbonate close to dolomite were not randomly
395 oriented, but rather followed the orientations of seed crystals and displayed low-angle grain
396 boundaries between neighboring nano-crystals **(Fig. 8c)**. The [010]-zone axis SAED and fast
397 Fourier transform (FFT) patterns did not show supper-lattice reflections like (003) and ($\bar{1}$05)
398 indicating the Ca-Mg cation order in dolomitic structure **(Fig. 8c, d)**. Thus our synthetic product
399 was disordered dolomite.

400 **Characterization of bound EPS**

401 Our analyses showed that the total polysaccharide content of the bound EPS was 8.4±0.5
402 wt%, that is, ~2.1 mg L^{-1} out of ~25 mg L^{-1} of bound EPS. The saccharide monomer analyses
403 showed that mannose (~36 mol%), ribose (~30 mol%), rhamnose (~15 mol%), xylose (~10
404 mol%), and glucose (~7 mol%) were the dominant saccharide monomers of the polysaccharides
405 in bound EPS **(Table 2)**.

This is the peer-reviewed, final accepted version for American Mineralogist, published by the Mineralogical Society of America.
The published version is subject to change. Cite as Authors (Year) Title. American Mineralogist, in press.
DOI: https://doi.org/10.2138/am-2020-7381. http://www.minsocam.org/

406

407 **DISCUSSION**

408 **EPS catalyzed crystallization of disordered dolomite**

409 In this study, the bound EPS was extracted with a procedure which utilized formaldehyde
410 and NaOH. This procedure can minimize the contamination by intracellular substances since
411 formaldehyde can fix the cell, and thus prevent cell lysis, by reacting with the amino, hydroxyl,
412 carboxyl and sulfhydryl function groups of proteins and nucleic acids of the cell membrane
413 (Nielsen and Jahn 1999; Liu and Fang 2002). Furthermore, the addition of NaOH can cause
414 many charged groups, such as carboxylic groups in proteins and polysaccharides to be
415 dissociated, which results in a strong repulsion between the negatively charged EPS and thus
416 provides a higher water solubility of the compounds. One question, however, is whether the use
417 of NaOH and the possible reaction between bound EPS and formaldehyde played a critical role
418 in disordered dolomite precipitation. The effect of NaOH should be easily excluded because the
419 NaOH was removed from the bound EPS solution during dialysis. Regarding the effect of
420 formaldehyde, since non-metabolizing consortium biomass which was not processed with
421 formaldehyde also catalyzed similar disordered dolomite precipitation as bound PES did, the
422 contribution from formaldehydeshould not be significant.

423 Our experimental data showed that a higher initial Mg:Ca ratio in solutions generally
424 results in higher $MgCO_3$ contents in precipitated Ca-Mg carbonates **(Fig. 4)**, which is consistent
425 with previous works on carbonate synthesis (Devery and Ehlmann 1981; Rushdi et al. 1992;
426 Zhang et al. 2012b). Therefore, we may speculate that the catalytic effect of bound EPS was a
427 result of increased Mg:Ca ratio in solution due to the binding of cations to bound EPS. That is, if
428 fewer Mg^{2+} is bound to bound EPS than Ca^{2+}, the initial Mg:Ca ratio in solution can be sharply

increased. To address this question, knowledge of the binding capacity of bound EPS of *M. barkeri* is essential. Unfortunately, we did not find such published data. Nevertheless, previous studies on the cation-binding capacity of soluble EPS extracted from SRB cultures may provide some clue (Braissant et al. 2007). A Ca-binding capacity of 0.12-0.15 g_{Ca}/g_{EPS} has been determined while no data for Mg is available. Although it is unlikely that the binding capacity of the bound EPS we collected is the same as that of Braissant et al. (2007), these numbers can still offer some first-order estimations. For example, if we assume a binding capacity of 0.15 $g_{Ca}\ g_{EPS}^{-1}$ and 0 $g_{Mg}\ g_{EPS}^{-1}$, the ~25 mg L^{-1} of bound EPS will bind 0.094 mM Ca^{2+}, resulting in an increase of Mg:Ca ratio from 3:1 to 3.06:1, from 4:1 to 4.08:1, from 5:1 to 5.1:1, from 8:1 to 8.15:1, respectively in our experiments. Such a small increase, which would be even smaller if bound EPS binds less Ca^{2+} and also binds Mg^{2+}, obviously cannot account for the huge enhancement of Mg incorporation by bound EPS.

In addition, although a definitive calculation was not available in this case, the saturation index of our experimental solutions with respect to disordered dolomite was presumably high. However, control solutions with even higher saturation index still did not produce disordered dolomite. Therefore a high saturation index cannot explain the bound EPS-induced crystallization of disordered dolomite.

Here, we suggest that polysaccharides are likely to be one of the catalytic components of bound EPS since polysaccharides have been shown to mediate calcite and disordered dolomite precipitation (Braissant et al. 2003; Bosak and Newman 2005; Kawano and Hwang 2011; Zhang et al. 2012b). For example, Mg-rich disordered dolomite crystallized in solutions containing ~200 mg L^{-1} of agar (Zhang et al. 2012b). Kawano and Hwang (2011) showed that polysaccharides can promote the precipitation of calcite while inhibiting aragonite crystallization.

This is the peer-reviewed, final accepted version for American Mineralogist, published by the Mineralogical Society of America.
The published version is subject to change. Cite as Authors (Year) Title. American Mineralogist, in press.
DOI: https://doi.org/10.2138/am-2020-7381. http://www.minsocam.org/

Braissant et al. (2003) found that purified exopolysaccharide (xanthan EPS) exerted a strong influence on the morphology of precipitated calcite. Our analyses showed that the total polysaccharide content of the bound EPS was 8.4 wt%, that is, ~2.1 mg L^{-1} out of ~25 mg L^{-1} of bound EPS. This concentration is much lower than the amount of agar required to trigger dolomite precipitation (Zhang et al. 2012b). This difference may be due simply to differences in the properties of polysaccharides in bound EPS compared to agar, given that the Mg-incorporation capacities can vary significantly among different polysaccharides. For comparison, disordered dolomite containing ~52 mol% of $MgCO_3$ crystallized in solutions containing ~200 mg L^{-1} of agar and an initial Mg:Ca ratio of 8:1, whereas ~5 g L^{-1} of carboxymethyl cellulose was required to produce such disordered dolomite under the same solution phase conditions (Zhang et al. 2012b). In this case, however, with only 25 mg L^{-1} of bound EPS, disordered dolomite containing ~48 mol% was precipitated in solution with an initial Mg:Ca ratio of 8:1. Therefore, it is not inconceivable that the small amounts of polysaccharides in the collected bound EPS of *M. barkeri* can catalyze disordered dolomite precipitation.

In addition to polysaccharides, the existence of other catalytic components in bound EPS should also be emphasized (Raz et al. 2000; Braissant et al. 2003; Gautret and Trichet 2005; Stephenson et al. 2008; Wang et al. 2009). For example, Raz et al. (2000) found that polyacrylic and polyaspartic acids can catalyze the crystallization of Ca-Mg carbonate with up to 34 mol% of $MgCO_3$. Stephenson et al (2008) showed that a small amount of peptides in solution can enhance the step velocity on the Ca-Mg carbonate growth hillock and slightly enhance Mg incorporation. Along analogous lines, carboxylated organic acids with a strong affinity for binding Ca^{2+} compared to Mg^{2+} were shown to promote the formation of Mg-enriched amorphous calcium carbonates (Wang et al. 2009). These possible catalytic components, along

475 with polysaccharides, may function synergistically to catalyze disordered dolomite nucleation
476 and growth.

477 In previous studies, the role of EPS in calcium carbonate and dolomite formation was
478 mostly attributed to their ability to provide nucleation sites (Warthmann et al. 2000; Van Lith et
479 al. 2003b, a; Roberts et al. 2004; Aloisi et al. 2006; Bontognali et al. 2008; Kenward et al. 2009;
480 Deng et al. 2010; Bontognali et al. 2014). For example, Aloisi et al. (2006) found that bacterial
481 nucleation of calcium carbonate in a SRB culture was initiated at the bound EPS as nano-
482 globules and these nano-globules calcified significantly only when released to the culture
483 medium. Aloisi et al. (2006) suggested that carbonate nucleation as nano-globules could be an
484 important step in microbial carbonate precipitation. Here we approach the concept of "nucleation
485 sites" from a different point of view. As our SEM and TEM data showed, it was the calcite seeds
486 in our experiments that provided sites for the heterogeneous nucleation of disordered dolomite.
487 However, this does not suggest that bound EPS was not involved. Instead, as in previous studies
488 (Zhang et al. 2012a; Zhang et al. 2012b), we propose that the EPS adsorbed onto Ca-Mg
489 carbonate surfaces through hydrogen bonding between the H in the OH group of bound EPS and
490 the O in the CO_3^{2-} on carbonate surfaces. This in turn displaced surface water molecules which
491 would otherwise be associated with the hydration shell of Mg^{2+}, thereby facilitating Mg
492 incorporation and disordered dolomite crystallization. In other words, the nucleation sites for
493 disordered dolomite provided by calcite seeds will be functional only with the adsorbed bound
494 EPS. This hypothesis is supported by the saccharide monomer analyses of the polysaccharides in
495 bound EPS. Our data showed that mannose (~36 mol%), ribose (~30 mol%), rhamnose (~15
496 mol%), xylose (~10 mol%), and glucose (~7 mol%) were the dominant saccharide monomers of
497 the polysaccharides in bound EPS. While there is no data for ribose and glucose, molecular

dynamic simulations showed that xylose, rhamnose and mannose have a stronger adsorption onto calcite (104) surfaces than water (Yang et al. 2008).

Our experiments with non-metabolizing biomass also succeeded in precipitating disordered dolomite. We suggest that bound EPS of the non-metabolizing biomass may have easily desorbed from the cell surface into the solution during the dialysis and the precipitation experiments due to the possible lysis of cells. For example, ultrasonication, which is also a common procedure used for EPS extraction (Nielsen and Jahn 1999), was used to suspend added calcite seed crystals in experimental solutions. The released bound EPS then can be adsorbed onto carbonate surfaces to promote the dehydration of surface Mg^{2+}.

DCP was also shown to slightly enhance Mg incorporation compared to control experiments **(Fig. 6; Table 1)**. One possibility of the effect of DCP is that the bound EPS was not totally striped from cell surface during extraction based on synthesized Ca-Mg-carbonates (Fig. 10). In addition, the thick cell wall of *M. barkeri* was probably another source where this catalytic effect was originated. Ultrathin sections showed a very thick (500 nm), amorphous outer layer of *M. barkeri*'s cell wall which often appeared laminated (Zeikus and Bowen 1975). Results of chemical analyses of isolated cell walls indicated that they consist of an acid heteropolysaccharide that contains galactosamine, neutral sugars, and uronic acids (Kandler and Hippe 1977; Balch et al. 1979). Therefore it is possible that the polysaccharides and some other components of the cell wall also exerted catalytic effect during carbonate precipitation.

Implications for the "dolomite problem"

As described above, our synthetic dolomite was finely crystalline, Ca-rich, and cation-disordered. It is most likely that the inhibitory effect of Mg^{2+} ions on dolomite growth resulted in the

extremely small size of dolomite crystals. Precipitation experiments with SRB also precipitated similar disordered dolomite (Bontognali et al. 2014). Modern dolomites associated with methanogenesis are also generally finely crystalline, Ca-rich and poorly ordered (Pisciotto and Mahoney 1981; Baker and Burns 1985; Compton and Siever 1986; Thornburg and Suess 1990; Mazzullo 2000; Roberts et al. 2004). With deposition, poorly-crystallized disordered dolomite can undergo maturation and recrystallization accompanied by increased cation ordering and crystallinity, which can produce partially ordered proto-dolomite and eventually, fully ordered dolomite (Lippmann 1973; Hardie 1987; Gregg et al. 1992; Vasconcelos and McKenzie 1997; Warren 2000). Thus disordered dolomite induced by the bound EPS of methanogens can be considered as a precursor to some sedimentary ordered dolomite. It was reported that the dolomite or protodolomite formed in the methanogenesis zone will have high $\delta^{13}C$ values (Mazzullo 2000; Greinert et al. 2001). The carbon isotope fractionation will enrich ^{13}C in bicarbonate and deplete ^{13}C in methane. The dolomite formed in this environment will have high $\delta^{13}C$ values, i.e., group A carbonate (Claypool and Kaplan 1974; Hennessy and Knauth 1985; Burns and Baker 1987; Greinert et al. 2001; Blattler et al. 2015). The dolomite or calcian dolomite formed in these areas generally contains small amounts of Fe(II) or $FeCO_3$. In extreme cases, even siderite can precipitate. The existence of Fe^{2+} in dolomite also indicates a reducing dolomitizing fluid that contains dissolved methane and other organics that are responsible for the dolomite precipitation. It has been shown that fermenting bacteria can transfer electrons to Fe(III) in sediments (Lovley 2000). The cooperative metabolism between methanogens and fermenting bacteria results in CO_2 or dissolved HCO_3^- as the common product of all these reactions which can result in Fe^{2+}-bearing carbonate (Coleman and Raiswell 1993).

This is the peer-reviewed, final accepted version for American Mineralogist, published by the Mineralogical Society of America.
The published version is subject to change. Cite as Authors (Year) Title. American Mineralogist, in press.
DOI: https://doi.org/10.2138/am-2020-7381. http://www.minsocam.org/

Although our results suggest a potential link between methanogens and dolomite formation, caution must be exercised in extrapolating laboratory data to explaining natural dolomite formation. First, no evidence has been shown to demonstrate the presence of *M. barkeri* or any other methanogens in natural dolomite formation. While there is a possibility that the correlation between natural dolomite formation and *M. barkeri* and other methanogens simply has not yet been recognized, there may be some other factors that are noteworthy. First, bound EPS excreted by microorganisms in laboratory cultures is unlikely to be the same with the EPS matrix produced by the same microorganisms in natural environments (Nielsen and Jahn 1999). The production of EPS likely follows an ecophysiological response and the chemical composition and 3-D architecture of the EPS can be greatly influenced by the growth conditions (Nielsen et al. 1997; Nielsen and Jahn 1999; Dupraz et al. 2009). In other words, considering the different Mg-incorporation capacities of various polysaccharides, amino acids, proteins, polycarboxylic acids, etc (see discussion above), the growth conditions in current experiments might have a significant impact on the strength of the bound EPS in catalysis. In fact, as mentioned above, previous laboratory studies showed that in high extracellular solute concentrations *M barkeri* will not produce EPS (Stadtman and Barker 1951; Sowers et al. 1993; Anderson et al. 2012). Therefore it is possible that in some natural environments, *M. barkeri* may produce EPS matrix that might not have sufficient Mg-incorporation capacities to induce (disordered) dolomite precipitation.

In addition, the pH and saturation index with respect to disordered dolomite in our forced carbonate precipitation experiments were presumably high compared to that of nature environments. While high pH and supersaturation conditions can be found in some evaporitic settings and saline or hypersaline environments (e.g., Wright 1999), dolomite precipitation was

found in a methanogenic freshwater aquifer with neutral pH and close to equilibrium conditions (Roberts et al. 2004). Although a high pH and superstation cannot necessarily lead to disordered dolomite precipitation (see discussion above), reasonable pH and supersaturation levels are still required to carbonate precipitation (Dupraz et al. 2009; Gallagher et al. 2012). In fact, the pH of our live *M. barkeri* culture dropped from an initial pH of 6.5-6.8 to ~5.2, which explains why no carbonate precipitation was found in the live culture. Gallagher et al. (2012) found that the utilization of different substrates by SRB resulted in different pH, alkalinity, and thereby supersaturation. Since *M. barkeri* is versatile and can utilize a variety of methanogenic substrates, the possibility exists that the metabolism of *M. barkeri* may result in different pH and supersaturation conditions to induce the precipitation of different carbonate phases or even limit carbonate precipitation. For example, in natural sediments, the major substrates for methanogenesis are acetate (CH_3COO^-) and H_2 (Lovley and Klug 1982) whose conversion to methane, unlike methanol (CH_3OH), would be expected to elevate (e.g. through consumption of H^+ or CO_2) rather than decrease solution pH:

$$CH_3COO^- + H^+ \rightarrow CH_4 + CO_2$$

$$H_2 + CO_2 \rightarrow CH_4 + 2H_2O$$

$$4CH_3OH \rightarrow 3CH_4 + CO_2 + 2H_2O$$

Regardless of these dissimilarities between our experimental conditions and natural environments, we propose that the physiochemical mechanism by which bound EPS of various SRB and methanogen species in laboratory cultures and EPS matrix in natural environments catalyze (disordered) dolomite precipitation should be similar. However, as discussed above, the strength in catalysis or the Mg-incorporation capacities of EPS can vary among different microorganism species or even in the same species when the growth conditions are different.

589

590

591 **IMPLICATIONS**

592 In this study, we characterized the effect of bound EPS of the methanogen *M. barkeri* on
593 Ca-Mg carbonate precipitation. Forced carbonate precipitation experiments at room temperature
594 in calcite-seeded Ca/Mg carbonate solutions showed that non-metabolizing biomass of *M.*
595 *Barkeri* can enhance the Mg incorporation into calcitic structure and induce the crystallization of
596 disordered dolomite. Bound EPS was shown to be the component of non-metabolizing biomass
597 that catalyzed the precipitation of disordered dolomite. We propose a mechanism to explain the
598 catalytic effect of bound EPS based on the adsorption of bound EPS to growing carbonate
599 surfaces through hydrogen bonding. This mechanism is also applicable to natural EPS-induced
600 dolomite formation. While our experimental conditions cannot completely mimic the natural
601 environments, this study contributes new insights into to the long-standing "dolomite problem",
602 especially the sedimentary dolomite with heavy $\delta^{13}C$ values. The formation of methane will
603 result in light carbon in methane phase and heavy carbon in aqueous carbonate that may be
604 incorporated into the carbonate mineral like dolomite in presence of the methanogens.

605

606

607 **ACKNOWLEDGEMENTS**

608 The authors acknowledge the financial support from NASA Astrobiology Institute (N07-
609 5489), NSF (EAR-095800), and U.S. Department of Energy (DE-SC0001929).

610

611

612 **REFERENCES**

613 Aloisi, G., Gloter, A., KrOger, M., Wallmann, K., Guyot, F., and Zuddas, P. (2006) Nucleation of
614 calcium carbonate on bacterial nanoglobules. Geology, 34(12), 1017-1020.
615 Anderson, K.L., Apolinario, E.E., and Sowers, K.R. (2012) Desiccation as a long-term survival
616 mechanism for the archaeon *Methanosarcina barkeri*. Applied and Environmental Microbiology,
617 78(5), 1473-1479.
618 Anovitz, L.M., and Essene, E.J. (1987) Phase-equilibria in the system $CaCO_3$-$MgCO_3$-$FeCO_3$. Journal of
619 Petrology, 28(2), 389-414.
620 Baker, P.A., and Burns, S.J. (1985) Occurrence and formation of dolomite in organic-rich continental
621 margin sediments. AAPG Bulletin, 69(11), 1917-1930.
622 Baker, P.A., and Kastner, M. (1981) Constraints on the formation of sedimentary dolomite. Science,
623 213(4504), 214-216.
624 Balch, W.E., Fox, G.E., Magrum, L.J., Woese, C.R., and Wolfe, R.S. (1979) Methanogens: Reevaluation
625 of a unique biological group. Microbiological Reviews, 43(2), 260-296.
626 Berner, R.A. (1975) The role of magnesium in the crystal growth of calcite and aragonite from sea water.
627 Geochimica et Cosmochimica Acta, 39(4), 489-494.
628 Blattler, C.L., Miller, N.R., and Higgins, J.A. (2015) Mg and Ca isotope signatures of authigenic dolomite
629 in siliceous deep-sea sediments. Earth and Planetary Science Letters, 419, 32-42.
630 Bock, C.W., Kaufman, A., and Glusker, J.P. (1994) Coordination of water to magnesium cations.
631 Inorganic Chemistry, 33(3), 419-427.
632 Bontognali, T.R., McKenzie, J.A., Warthmann, R.J., and Vasconcelos, C. (2014) Microbially influenced
633 formation of Mg-calcite and Ca-dolomite in the presence of exopolymeric substances produced
634 by sulphate-reducing bacteria. Terra Nova, 26(1), 72-77.
635 Bontognali, T.R.R., Vasconcelos, C., Warthmann, R.J., Bernasconi, S.M., Dupraz, C., Strohmenger, C.J.,
636 and McKenzie, J.A. (2010) Dolomite formation within microbial mats in the coastal sabkha of
637 Abu Dhabi (United Arab Emirates). Sedimentology, 57(3), 824-844.
638 Bontognali, T.R.R., Vasconcelos, C., Warthmann, R.J., Dupraz, C., Bernasconi, S.M., and McKenzie, J.A.
639 (2008) Microbes produce nanobacteria-like structures, avoiding cell entombment. Geology, 36(8),
640 663-666.
641 Bosak, T., and Newman, D.K. (2005) Microbial kinetic controls on calcite morphology in supersaturated
642 solutions. Journal of Sedimentary Research, 75(2), 190-199.
643 Braissant, O., Cailleau, G., Dupraz, C., and Verrecchia, A.P. (2003) Bacterially induced mineralization of
644 calcium carbonate in terrestrial environments: The role of exopolysaccharides and amino acids.
645 Journal of Sedimentary Research, 73(3), 485-490.

646 Braissant, O., Decho, A.W., Dupraz, C., Glunk, C., Przekop, K.M., and Visscher, P.T. (2007)
647 Exopolymeric substances of sulfate-reducing bacteria: Interactions with calcium at alkaline pH
648 and implication for formation of carbonate minerals. Geobiology, 5(4), 401-411.
649 Brunauer, S., Emmett, P.H., and Teller, E. (1938) Adsorption of gases in multimolecular layers. Journal
650 of American Chemical Society, 60(2), 309-319.
651 Burdige, D.J., Skoog, A., and Gardner, K. (2000) Dissolved and particulate carbohydrates in contrasting
652 marine sediments. Geochimica et Cosmochimica Acta, 64(6), 1029-1041.
653 Burns, S.J., and Baker, P.A. (1987) A GEOCHEMICAL STUDY OF DOLOMITE IN THE MONTEREY
654 FORMATION, CALIFORNIA. Journal of Sedimentary Petrology, 57(1), 128-139.
655 Burns, S.J., McKenzie, J.A., and Vasconcelos, C. (2000) Dolomite formation and biogeochemical cycles
656 in the Phanerozoic. Sedimentology, 47, 49-61.
657 Capo, R.C., Whipkey, C.E., Blachère, J.R., and Chadwick, O.A. (2000) Pedogenic origin of dolomite in a
658 basaltic weathering profile, Kohala peninsula, Hawaii. Geology, 28(3), 271-274.
659 Carpenter, A.B. (1980) The chemistry of dolomite formation I: The stability of dolomite. In D.H. Zenger,
660 J.B. Dunham, and R.L. Ethington, Eds. Concepts and Models of Dolomitization, p. 111-121.
661 SEPM Specical Publication 28, Tulsa.
662 Chan, C.S., De Stasio, G., Welch, S.A., Girasole, M., Frazer, B.H., Nesterova, M.V., Fakra, S., and
663 Banfield, J.F. (2004) Microbial polysaccharides template assembly of nanocrystal fibers. Science,
664 303(5664), 1656-1658.
665 Claypool, G., and Kaplan, I.R. (1974) The origin and distribution of methane in marine sediments.
666 Natural Gases in Marine Sediments, p. 99-139. Springer.
667 Coleman, M.L., and Raiswell, R. (1993) Microbial mineralization of organic-matter-mechanisms of self-
668 organization and inferred rates of precipitiation of diagenetic minerals. Philosophical
669 Transactions of the Royal Society of London Series a-Mathematical Physical and Engineering
670 Sciences, 344(1670), 69-87.
671 Colson, J., and Cojan, I. (1996) Groundwater dolocretes in a lake-marginal environment: An alternative
672 model for dolocrete formation in continental settings (Danian of the Provence Basin, France).
673 Sedimentology, 43(1), 175-188.
674 Compton, J.S. (1988) Degree of supersaturation and precipitation of organogenic solomite. Geology,
675 16(4), 318-321.
676 Compton, J.S., and Siever, R. (1986) Diffusion and mass balance of Mg during early dolomite formation,
677 Monterey Formation. Geochimica et Cosmochimica Acta, 50(1), 125-135.
678 Costerton, J.W., Lewandowski, Z., Caldwell, D.E., Korber, D.R., and Lappin-Scott, H.M. (1995)
679 Microbial biofilms. Annual Review of Microbiology, 49(1), 711-745.

680 Deng, S., Dong, H., Lv, G., Jiang, H., Yu, B., and Bischoff, M.E. (2010) Microbial dolomite precipitation
681 using sulfate reducing and halophilic bacteria: Results from Qinghai Lake, Tibetan Plateau, NW
682 China. Chemical Geology, 278(3-4), 151-159.
683 Devery, D.M., and Ehlmann, A.J. (1981) Morphological changes in a series of synthetic Mg-calcites.
684 American Mineralogist, 66(5-6), 592-595.
685 Dubois, M., Gilles, K.A., Hamilton, J.K., Rebers, P.A., and Smith, F. (1956) Colorimetric method for
686 determination of sugars and related substances. Analytical Chemistry, 28(3), 350-356.
687 Dupraz, C., Reid, R.P., Braissant, O., Decho, A.W., Norman, R.S., and Visscher, P.T. (2009) Processes of
688 carbonate precipitation in modern microbial mats. Earth-Science Reviews, 96(3), 141-162.
689 Dupraz, C., and Visscher, P.T. (2005) Microbial lithification in marine stromatolites and hypersaline mats.
690 Trends in Microbiology, 13(9), 429-438.
691 Dupraz, C., Visscher, P.T., Baumgartner, L.K., and Reid, R.P. (2004) Microbe-mineral interactions: early
692 carbonate precipitation in a hypersaline lake (Eleuthera Island, Bahamas). Sedimentology, 51(4),
693 745-765.
694 El-Sayed, M.I., Fairchild, I.J., and Spiro, B. (1991) Kuwaiti dolocrete: petrology, geochemistry and
695 groundwater origin. Sedimentary Geology, 73(1), 59-75.
696 Fang, Y., and Xu, H. (2019) A new approach to quantify ordering state of protodolomite using
697 XRD, TEM, and Z-contrast imaging. Journal of Sedimentary Research, 89, 537–551.
698 Fortin, D., Ferris, F.G., and Beveridge, T.J. (1997) Surface-mediated mineral development by bacteria. In
699 J.F. Banfield, and K.H. Nealson, Eds. Geomicrobiology: Interactions between Microbes and
700 Minerals, 35, p. 161-180. Mineralogical Society of America, Washington, D.C.
701 Gallagher, K.L., Braissant, O., Kading, T.J., Dupraz, C., and Visscher, P.T. (2013) Phosphate-Related
702 Artifacts In Carbonate Mineralization Experiments. Journal of Sedimentary Research, 83(1), 37-
703 49.
704 Gallagher, K.L., Kading, T.J., Braissant, O., Dupraz, C., and Visscher, P.T. (2012) Inside the alkalinity
705 engine: the role of electron donors in the organomineralization potential of sulfate-reducing
706 bacteria. Geobiology, 10(6), 518-530.
707 Gautret, P., and Trichet, J. (2005) Automicrites in modern cyanobacterial stromatolitic deposits of
708 Rangiroa, Tuamotu Archipelago, French Polynesia: Biochemical parameters underlaying their
709 formation. Sedimentary Geology, 178(1), 55-73.
710 Geesey, G.G., Jang, L., Jolley, J.G., Hankins, M.R., Iwaoka, T., and Griffiths, P.R. (1988) Binding of
711 metal ions by extracellular polymers of biofilm bacteria. Water Science and Technology, 20(11-
712 12), 161-165.

713 Gregg, J.M., Howard, S.A., and Mazzullo, S.J. (1992) Early diagenetic recrystallization of. Holocene (<
714 3000 years old) peritidal dolomites, Ambergris Cay, Belize. Sedimentology, 39(1), 143-160.
715 Greinert, J., B., B., and Suess, E. (2001) Gas hydrate-associated carbonates and methane-venting at
716 Hydrate ridge : Classification, distribution, and origin of authigenic lithologies. In C.K.P.a.W.P.
717 Dillon, Ed. Natural Gas Hydrates: Occurrence, Distribution, and Detection, p. 99-113. American
718 Geophysical Union, Washington, DC.
719 Hardie, L.A. (1987) Dolomitization - a critical view of some current views. Journal of Sedimentary
720 Research, 57(1), 166-183.
721 Harrison, J.J., Ceri, H., and Turner, R.J. (2007) Multimetal resistance and tolerance in microbial biofilms.
722 Nature Reviews Microbiology, 5(12), 928-938.
723 Hennessy, J., and Knauth, L.P. (1985) ISOTOPIC VARIATIONS IN DOLOMITE CONCRETIONS
724 FROM THE MONTEREY FORMATION, CALIFORNIA. Journal of Sedimentary Petrology,
725 55(1), 120-130.
726 Higgins, S.R., and Hu, X.M. (2005) Self-limiting growth on dolomite: Experimental observations with in
727 situ atomic force microscopy. Geochimica et Cosmochimica Acta, 69(8), 2085-2094.
728 Hippe, H., Caspari, D., Fiebig, K., and Gottschalk, G. (1979) Utilization of trimethylamine and other *N*-
729 methyl compounds for growth and methane formation by *Methanosarcina barkeri*. Proceedings
730 of the National Academy of Sciences, 76(1), 494-498.
731 Hsieh, K.M., Murgel, G.A., Lion, L.W., and Shuler, M.L. (1994) Interactions of microbial biofilms with
732 toxic trace metals: 1. Observation and modeling of cell growth, attachment, and production of
733 extracellular polymer. Biotechnology and Bioengineering, 44(2), 219-231.
734 Jones, B.F. (1961) Zoning of saline minerals at Deep Springs Lake. Short Papers in the Geological
735 Sciences: US Geological Survey Professional Paper 421, B199-B202.
736 Kandler, O., and Hippe, H. (1977) Lack of peptidoglycan in the cell walls of *Methanosarcina barkeri*.
737 Archives of Microbiology, 113(1), 57-60.
738 Kawaguchi, T., and Decho, A.W. (2002) Isolation and biochemical characterization of extracellular
739 polymeric secretions (EPS) from modern soft marine stromatolites (Bahamas) and its inhibitory
740 effect on CaCO3 precipitation. Preparative Biochemistry and Biotechnology, 32(1), 51-63.
741 Kawano, M., and Hwang, J. (2011) Roles of microbial acidic polysaccharides in precipitation rate and
742 polymorph of calcium carbonate minerals. Applied Clay Science, 51(4), 484-490.
743 Kenward, P.A., Goldstein, R.H., Gonzalez, L.A., and Roberts, J.A. (2009) Precipitation of low-
744 temperature dolomite from an anaerobic microbial consortium: the role of methanogenic Archaea.
745 Geobiology, 7(5), 556-565.

Krause, S., Liebetrau, V., Gorb, S., Sánchez-Román, M., McKenzie, J.A., and Treude, T. (2012) Microbial nucleation of Mg-rich dolomite in exopolymeric substances under anoxic modern seawater salinity: New insight into an old enigma. Geology, 40(7), 587-590.

Land, L.S. (1998) Failure to precipitate dolomite at 25 ^{o}C from dilute solution despite 1000-fold oversaturation after 32 years. Aquatic Geochemistry, 4(3-4), 361-368.

Laspidou, C.S., and Rittmann, B.E. (2002) A unified theory for extracellular polymeric substances, soluble microbial products, and active and inert biomass. Water Research, 36(11), 2711-2720.

Li, P., Liu, Z., and Xu, R. (2001) Chemical characterisation of the released polysaccharide from the cyanobacterium Aphanothece halophytica GR02. Journal of Applied Phychology, 13(1), 71-77.

Lian, B., Hu, Q., Chen, J., Ji, J., and Teng, H.H. (2006) Carbonate biomineralization induced by soil bacterium *Bacillus megaterium*. Geochimica et Cosmochimica Acta, 70(22), 5522-5535.

Lippmann, F. (1973) Sedimentary Carbonate Minerals. 228 p. Springer, New York.

Liu, D., Xu, Y., Papineau, D., Yu, N., Fan, Q., Qiu, X., and Wang, H. (2019) Experimental evidence for abiotic formation of low-temperature proto-dolomite facilitated by clay minerals. Geochimica et Cosmochimica Acta, 247, 83–95.

Liu, H., and Fang, H.H.P. (2002) Extraction of extracellular polymeric substances (EPS) of sludges. Journal of Biotechnology, 95(3), 249-256.

Lovley, D.R. (2000) Fe(III) and Mn(IV) reduction. In D.R. Lovley, Ed. Environmental Microbe-metal Interactions, p. 3030. ASM Press, Washington, D. C.

Machel, H.G., and Mountjoy, E.W. (1986) Concepts and models of dolomitization: a critical reappraise. Earth-Science Reviews, 23(3), 175-222.

Maeder, D.L., Anderson, I., Brettin, T.S., Bruce, D.C., Gilna, P., Han, C.S., Lapidus, A., Metcalf, W.W., Saunders, E., Tapia, R., and Sowers, K.R. (2006) The *Methanosarcina barkeri* genome: Comparative analysis with with *Methanosarcina acetivorans* and *Methanosarcina mazei* reveals extensive rearrangement within *Methanosarcinal* genomes. Journal of Bacteriology, 188(22), 7922-7931.

Mazzullo, S.J. (2000) Organogenic dolomitization in peritidal to deep-sea sediments. Journal of Sedimentary Research, 70(1), 10-23.

Merkle, R.K., and Poppe, I. (1994) Carbohydrate composition analysis of glycoconjugates by gas-liquid chromatography/mass spectrometry. Methods in Enzymology, 230, 1-15.

Nielsen, P.H., and Jahn, A. (1999) Extraction of EPS. In J. Wingender, T.R. Neu, and H.-C. Flemming, Eds. Microbial Extracellular Polymeric Substances, p. 49-72. Springer, Berlin.

778 Nielsen, P.H., Jahn, A., and Palmgren, R. (1997) Conceptual model for production and composition of
779 exopolymers in biofilms. Water Science and Technology, 36(1), 11-19.
780 Oomori, T., and Kitano, Y. (1987) Synthesis of protodolomite from sea-water containing dioxane.
781 Geochemical Journal, 21(2), 59-65.
782 Ortega-Morales, B.O., Santiago-García, J.L., Chan-Bacab, M.J., Moppert, X., Miranda-Tello, E., Fardeau,
783 M.L., Carrero, J.C., Bartolo-Pérez, P., Valadéz-González, A., and Guezennec, J. (2006)
784 Characterization of extracellular polymers synthesized by tropical intertidal biofilm bacteria.
785 Journal of Applied Microbiology, 102(1), 254-264.
786 Pakulski, J.D., and Benner, R. (1992) An improved method for the hydrolysis and MBTH analysis of
787 dissolved and particulate carbohydrates in seawater. Marine Chemistry, 40(3-4), 143-160.
788 Parkhurst, D.L., and Appelo, C.A.J. (1999) User's guide to PHREEQC (Version 2)–A computer program
789 for speciation, batch-reaction, one-dimensional transport, and inverse geochemical calculations,
790 Water-Resources Investigations Report 99-4259. US Geological Survey, Denver, CO.
791 Paulo, C., and Dittrich, M. (2013) 2D Raman spectroscopy study of dolomite and cyanobacterial
792 extracellular polymeric substances from Khor Alâ€• Adaid sabkha (Qatar). Journal of Raman
793 Spectroscopy, 44(11), 1563-1569.
794 Perry, T.D., Klepac-Ceraj, V., Zhang, X.V., McNamara, C.J., Polz, M.F., Martin, S.T., Berke, N., and
795 Mitchell, R. (2005) Binding of harvested bacterial exopolymers to the surface of calcite.
796 Environmental Science & Technology, 39(22), 8770-8775.
797 Pisciotto, K.A., and Mahoney, J.J. (1981) Isotopic survey of diagenetic carbonates, Deep Sea Drilling
798 Project Leg 63. Initial Reports of Deep Sea Drilling Project, 63, 595-609.
799 Pursher, B.H., Tucker, M., and Zenger, D.H. (1994) Problems, progress and future research concerning
800 dolomite and dolomitization. In B.H. Pursher, M. Tucker, and D.H. Zenger, Eds. Dolomites., 21
801 of Spec. Publs. int. Ass. Sediment., p. 3-20. Blackwell, Oxford.
802 Raz, S., Weiner, S., and Addadi, L. (2000) Formation of high-magnesian calcites via an amorphous
803 precursor phase: Possible biological implications. Advanced Materials, 12(1), 38-42.
804 Reid, R.P., Visscher, P.T., Decho, A.W., Stolz, J.F., Bebout, B.M., Dupraz, C., Macintyre, I.G., Paerl,
805 H.W., Pinckney, J.L., and Prufert-Bebout, L. (2000) The role of microbes in accretion, lamination
806 and early lithification of modern marine stromatolites. Nature, 406(6799), 989-992.
807 Roberts, J.A., Bennett, P.C., Gonzalez, L.A., Macpherson, G.L., and Milliken, K.L. (2004) Microbial
808 precipitation of dolomite in methanogenic groundwater. Geology, 32(4), 277-280.
809 Rushdi, A.I., Pytkowicz, R.M., Suess, E., and Chen, C.T. (1992) The effects of magnesium-to-calcium
810 ratios in artificial seawater, at different Ionic products, upon the induction time, and the
811 mineralogy of calcium-carbonate: a laboratory study. Geological Rundschau, 81(2), 571-578.

812 Shen, Z., Szlufarska, I., Brown, P.E., and Xu, H. (2015) Investigation of the Role of
813 Polysaccharide in the Dolomite Growth at Low Temperature by Using Atomistic
814 Simulations. Langmuir, 31, 10435–10442.

815

816 Sowers, K.R., Boone, J.E., and Gunsalus, R.P. (1993) Disaggregation of *Methanosarcina* spp. and growth
817 as single cells at elevated osmolarity. Applied and Environmental Microbiology, 59(11), 3832-
818 3839.
819 Stadtman, T.C., and Barker, H.A. (1951) Studies on the methane fermentation IX. The origin of methane
820 in the acetate and methanol fermentations by *Methanosarcina*. Journal of Bacteriology, 61(1), 81-
821 86.
822 Stephenson, A.E., DeYoreo, J.J., Wu, L., Wu, K.J., Hoyer, J., and Dove, P.M. (2008) Peptides enhance
823 magnesium signature in calcite: Insights into origins of vital effects. Science, 322(5902), 724-727.
824 Thornburg, T.M., and Suess, E. (1990) Carbonate cementation of granular and fracture porosity:
825 Implications for the Cenozoic hydrologic development of the Peru continental margin.
826 Proceedings of the Ocean Drilling Program-Scientific Results, 112, 95-109.
827 Van Lith, Y., Warthmann, R., Vasconcelos, C., and McKenzie, J.A. (2003a) Microbial fossilization in
828 carbonate sediments: a result of the bacterial surface involvement in dolomite precipitation.
829 Sedimentology, 50(2), 237-245.
830 -. (2003b) Sulphate-reducing bacteria induce low-temperature Ca-dolomite and high Mg-calcite formation.
831 Geobiology, 1(1), 71-79.
832 Vasconcelos, C., and McKenzie, J.A. (1997) Microbial mediation of modern dolomite precipitation and
833 diagenesis under anoxic conditions (Lagoa Vermelha, Rio de Janeiro, Brazil). Journal of
834 Sedimentary Research, 67(3), 378-390.
835 Vasconcelos, C., McKenzie, J.A., Bernasconi, S., Grujic, D., and Tien, A.J. (1995) Microbial mediation
836 as a possible mechanism for natural dolomite formation at low-temperatures. Nature, 377(6546),
837 220-222.
838 Wang, D., Wallace, A.F., De Yoreo, J.J., and Dove, P.M. (2009) Carboxylated molecules regulate
839 magnesium content of amorphous calcium carbonates during calcification. Proceedings of the
840 National Academy of Sciences USA, 106(51), 21511-21516.
841 Warren, J. (2000) Dolomite: occurrence, evolution and economically important associations. Earth-
842 Science Reviews, 52(1-3), 1-81.

Warthmann, R., van Lith, Y., Vasconcelos, C., McKenzie, J.A., and Karpoff, A.M. (2000) Bacterially induced dolomite precipitation in anoxic culture experiments. Geology, 28(12), 1091-1094.

Whipkey, C.E., Capo, R.C., Hsieh, J.C.C., and Chadwick, O.A. (2002) Development of magnesian carbonates in Quaternary soils on the Island of Hawaii. Journal of Sedimentary Research, 72(1), 158-165.

Whitman, W.B., Ankwanda, E., and Wolfe, R.S. (1982) Nutrition and carbon metabolism of *Methanococcus voltae*. Journal of Bacteriology, 149(3), 852-863.

Wingender, J., Neu, T.R., and Flemming, H.-C. (1999) What are Bacterial Extracellular Polymeric Substances? In J. Wingender, T.R. Neu, and H.-C. Flemming, Eds. Microbial Extracellular Polymeric Substances, p. 1-15. Springer, Berlin.

Wolin, E.A., Wolin, M.J., and Wolfe, R.S. (1963) Formation of methane by bacterial extracts. The Journal of Biological Chemistry, 238, 2882-2886.

Wright, D.T. (1999) The role of sulphate-reducing bacteria and cyanobacteria in dolomite formation in distal ephemeral lakes of the Coorong region, South Australia. Sedimentary Geology, 126(1-4), 147-157.

Wright, D.T., and Wacey, D. (2005) Precipitation of dolomite using sulphate-reducing bacteria from the Coorong Region, South Australia: significance and implications. Sedimentology, 52(5), 987-1008.

Xu, H. (2010) Synergistic roles of microorganisms in mineral precipitates acssociated with deep sea methane seeps. In Loy, Alexander, Mandl, Martin, Barton, Larry L. (Eds.) "Geomicrobiology: Molecular and Environmental Perspective." pp. 325–346, Springer.

Xu, H., Zhou, M., Fang, Y., and Teng, H.H. (2018) Effect of mica and hematite (001) Surfaces on the precipitation of calcite. Minerals, 8(1), 17; https://doi.org/10.3390/min8010017.

Xu, J., Campbell, J.M., Zhang, N., Hickey, W.J., and Sahai, N. (2012) Did mineral surface chemistry and toxicity contribute to evolution of microbial extracellular polymeric substances? Astrobiology, 12(8), 785-798.

Xu, J., Yan, C., Zhang, F., Konishi, H., Xu, H., and Teng, H.H. (2013) Testing the cation-hydration effect on the crystallization of Ca-Mg-CO_3 systems. Proceedings of the National Academy of Sciences USA, 110(44), 17750-17755.

Yang, M.J., Stipp, S.L.S., and Harding, J. (2008) Biological control on calcite crystallization by polysaccharides. Crystal Growth and Design, 8(11), 4066-4074.

York, W.S., Darvill, A.G., McNeil, M., Stevenson, T.T., and Albersheim, P. (1986) Isolation and characterization of plant cell walls and cell wall components. Methods in Enzymology, 118, 3-40.

875 Zeikus, J.G., and Bowen, V.G. (1975) Comparative ultrastructure of methanogenic bacteria. Canadian
876 Journal of Microbiology, 21(2), 121-129.
877 Zenger, D.H., Dunham, J.B., and Ethington, R.L. (1980) Concepts and Models of Dolomitization. 320 p.
878 SEM, Tulsa.
879 Zhang, F., Xu, H., Konishi, H., Kemp, J.M., Roden, E.E., and Shen, Z. (2012a) Dissolved sulfide-
880 catalyzed precipitation of disordered dolomite: Implications for the formation mechanism of
881 sedimentary dolomite. Geochimica et Cosmochimica Acta, 97, 148-165.
882 Zhang, F., Xu, H., Konishi, H., and Roden, E.E. (2010) A relationship between d_{104} value and
883 composition in the calcite - disordered dolomite solid solution series. American Mineralogist,
884 95(11-12), 1650-1656.
885 Zhang, F., Xu, H., Konishi, H., Shelobolina, E.S., and Roden, E.E. (2012b) Polysaccharide-catalyzed
886 nucleation and growth of disordered dolomite: A potential precursor of sedimentary dolomite.
887 American Mineralogist, 97(4), 556-567.
888 Zhang, F., Yan, C., Teng, H.H., Roden, E.E., and Xu, H. (2013) *In situ* AFM observations of Ca–Mg
889 carbonate crystallization catalyzed by dissolved sulfide: Implications for sedimentary dolomite
890 formation. Geochimica et Cosmochimica Acta, 105, 44-55.

891 Zhang, F., Xu, H., Shelobolina, E.S., Konishi, H., Converse, B., Shen, Z., and Roden, E.E., 2015,
892 The catalytic effect of bound extracellular polymeric substances excreted by anaerobic
893 microorganisms on Ca-Mg carbonate precipitation: Implications for the “dolomite
894 problem”: American Mineralogist, v. 100, no. 2–3, p. 483–494.

This is the peer-reviewed, final accepted version for American Mineralogist, published by the Mineralogical Society of America.
The published version is subject to change. Cite as Authors (Year) Title. American Mineralogist, in press.
DOI: https://doi.org/10.2138/am-2020-7381. http://www.minsocam.org/

Table 1 Chemical conditions employed in carbonate precipitation experiments with the non-metabolizing biomass, bound EPS, and DCP and compositions of synthetic carbonates. Errors represent standard deviation.

Experiments	Initial Ca^{2+} (mM)	Initial Mg^{2+} (mM)	Initial pH	Final pH	Initial SI_{dd}*	Final Ca^{2+} (mM)	Final Mg^{2+} (mM)	Change in Mg^{2+} (mM)†	Final SI_{dd}*	$MgCO_3$ content based on d_{104} (mol%)‡
Control	5.2±0.2	15.0±0.2	7.8	9.3	5.29	0.05±0.01	14.6±0.2	0.4	3.34	7±1
	5.2±0.2	20.6±0.3	7.8	9.2	5.36	0.09±0.03	20.1±0.3	0.5	3.65	9.1±0.8
	5.2±0.2	24.8±0.1	7.8	9.2	5.39	0.14±0.01	24.2±0.2	0.6	3.87	11.9±0.7
	5.2±0.2	40.5±0.3	7.9	9.2	5.44	0.19±0.01	39.5±0.3	1.0	4.04	18±1
Non-metabolizing Biomass (65±7 mg L^{-1})	5.19±0.08	15.3±0.3	8.1	9.1	-	0.07±0.03	15.0±0.4	0.3	-	5.1±0.6
	5.19±0.08	21.7±0.4	8.2	9.1	-	0.09±0.02	21.0±0.5	0.7	-	12±1.3
	5.19±0.08	26.7±0.7	8.2	9.1	-	0.13±0.03	24.7±0.6	2.0	-	30±1.7
	5.19±0.08	43.0±1.2	8.2	9.2	-	1.05±0.08	40.6±0.6	2.4	-	32±2.1
Non-metabolizing Biomass (113±12 mg L^{-1})	5.1±0.1	15.7±0.3	8.0	9.1	-	0.14±0.04	15.3±0.3	0.4	-	5.7±0.1
	5.1±0.1	20.9±0.4	8.1	9.1	-	0.17±0.04	20.0±0.3	0.9	-	14±1.1
	5.1±0.1	26.5±0.6	8.0	9.0	-	0.20±0.02	23.3±0.5	3.2	-	41±1.3
	5.1±0.1	43.0±1.0	8.1	9.1	-	0.88±0.03	39.9±0.6	3.1	-	45±2.3
Non-metabolizing Biomass (161±17 mg L^{-1})	5.0±0.2	16.0±0.2	7.2	9.0	-	0.14±0.01	14.4±0.3	1.6	-	26±1.1
	5.0±0.2	22.1±0.6	7.4	9.0	-	0.18±0.03	18.1±0.7	4.0	-	42.3±0.3
	5.0±0.2	27.2±0.6	7.5	9.0	-	0.24±0.04	24.5±0.8	2.7	-	48.9±0.6
	5.0±0.2	42.9±0.2	7.5	9.1	-	1.4±0.2	41.1±0.2	1.8	-	-
Bound EPS (25±7 mg L^{-1})	5.0±0.1	15.2±0.5	6.7	9.1	-	0.05±0.01	14.9±0.4	0.3	-	5.4±0.6
	5.0±0.1	20.5±0.4	6.8	9.1	-	0.13±0.01	18.1±0.7	2.4	-	30±2.9
	5.0±0.1	26.1±0.7	7.0	9.0	-	0.16±0.02	22.7±0.7	3.4	-	47±2.1
	5.0±0.1	42.1±0.5	7.1	9.0	-	0.28±0.01	38.1±0.6	4.0	-	48±0.8
DCP (95±9 mg L^{-1})	4.9±0.1	14.8±0.2	6.8	8.9	-	0.23±0.01	14.5±0.4	0.3	-	3.0±1.1
	4.9±0.1	20.4±0.1	6.8	8.9	-	0.12±0.04	19.7±0.4	0.7	-	10±1.6
	4.9±0.1	26.7±0.5	7.1	8.9	-	0.08±0.01	25.9±0.5	0.8	-	15±2
	4.9±0.1	42.4±0.6	7.1	8.9	-	0.06±0.01	39.1±0.3	3.3	-	25±2 and 46±2¶

*Initial and final SI with respect to disordered dolomite. See text for calculation details.
†The difference between initial and final Mg^{2+} concentration.
‡Molar content of $MgCO_3$ in synthetic Ca-Mg carbonates based on the Zhang et al. (2010) curve.
¶Two phases of Ca-Mg carbonate were identified in these precipitates.

897 **Table 2** Analysis of the monosaccharide composition in the polysaccharide fraction of bound
898 EPS.

899

	mol%
Mannose	36
Ribose	30
Rhamnose	15
Xylose	10
Glucose	7
Fructose	1
Glucuronic acid	1

Figures' captions

Fig. 1. XRD patterns of synthetic Ca–Mg carbonates induced by inactive biomass of *M. barkeri* (113±12 mg/L). Synthetic calcite (0.2 g/L) was used as seed crystals. Peaks correspond to: A: aragonite; C: calcite seeds; D: Ca-dolomite; H: HMC.

(a): HMC (d_{104} = 3.0192 Å, 5.6 mol% of $MgCO_3$) synthesized in inactive biomass-bearing solutions (Mg:Ca = 3:1). A small amount of aragonite was identified in precipitates.

(b): HMC (d_{104} = 2.9926 Å, 15.0 mol% of $MgCO_3$) synthesized in inactive biomass-bearing solutions (Mg:Ca = 4:1). A small amount of aragonite was identified in precipitates.

(c): Ca-dolomite (d_{104} = 2.9388 Å, 41.8 mol% of $MgCO_3$) synthesized in inactive biomass-bearing solutions (Mg:Ca = 5:1).

(d): Ca-dolomite (d_{104} = 2.9305 Å, 46.7 mol% of $MgCO_3$) synthesized in inactive biomass-bearing solutions (Mg:Ca = 8:1).

Fig. 2. XRD patterns of synthetic HMC from control experiments with synthetic calcite seeds (0.2 g/L). Peaks correspond to: A: aragonite; C: synthetic calcite; H: HMC.

(a): Aragonite and HMC (d_{104} = 3.0128 Å, 8.4 mol% $MgCO_3$) synthesized in control solutions (Mg:Ca = 3:1).

(b): Aragonite and HMC (d_{104} = 3.0078 Å, 9.5 mol% $MgCO_3$) synthesized in control solutions (Mg:Ca = 4:1).

(c): Aragonite and HMC (d_{104} = 3.0027 Å, 11.5 mol% $MgCO_3$) synthesized in control solutions (Mg:Ca = 5:1).

(d): Aragonite and HMC (d_{104} = 2.9831 Å, 18.5 mol% $MgCO_3$) synthesized in control solutions (Mg:Ca = 8:1).

This is the peer-reviewed, final accepted version for American Mineralogist, published by the Mineralogical Society of America.
The published version is subject to change. Cite as Authors (Year) Title. American Mineralogist, in press.
DOI: https://doi.org/10.2138/am-2020-7381. http://www.minsocam.org/

Fig. 3. XRD patterns of synthetic Ca–Mg carbonates induced by inactive biomass of *M. barkeri* (65±7 mg/L). Synthetic calcite (0.2 g/L) was used as seed crystals. Peaks correspond to: A: aragonite; C: calcite seeds; H: HMC.

(a): HMC (d_{104} = 3.0215 Å, 4.7 mol% of $MgCO_3$) synthesized in inactive biomass-bearing solutions (Mg:Ca = 3:1). A small amount of aragonite was identified in precipitates.

(b): HMC (d_{104} = 3.0004 Å, 12.5 mol% of $MgCO_3$) synthesized in inactive biomass-bearing solutions (Mg:Ca = 4:1). A small amount of aragonite was identified in precipitates.

(c): HMC (d_{104} = 2.9590 Å, 28.6 mol% of $MgCO_3$) synthesized in inactive biomass-bearing solutions (Mg:Ca = 5:1).

(d): HMC (d_{104} = 2.9568 Å, 30.0 mol% of $MgCO_3$) synthesized in inactive biomass-bearing solutions (Mg:Ca = 8:1).

Fig. 4. XRD patterns of synthetic Ca–Mg carbonates induced by inactive biomass of *M. barkeri* (161±17 mg/L). Synthetic calcite (0.2 g/L) was used as seed crystals. Peaks correspond to: A: aragonite; C: calcite seeds; D: Ca-dolomite; H: HMC; M: monohydrocalcite.

(a): HMC (d_{104} = 2.9611 Å, 26.7 mol% of $MgCO_3$) synthesized in inactive biomass-bearing solutions (Mg:Ca = 3:1). A small amount of monohydrocalcite was observed in precipitates.

(b): Ca-dolomite (d_{104} = 2.9373 Å, 42.7 mol% of $MgCO_3$) synthesized in inactive biomass-bearing solutions (Mg:Ca = 4:1). Monohydrocalcite was identified in precipitates.

(c): Ca-dolomite (d_{104} = 2.9256 Å, 49.3 mol% of $MgCO_3$) synthesized in inactive biomass-bearing solutions (Mg:Ca = 5:1). Monohydrocalcite was identified in precipitates.

(d): No crystalline Ca–Mg carbonate precipitation was observed in inactive biomass-bearing solutions (Mg:Ca = 8:1). Monohydrocalcite was identified in precipitates.

Fig. 5. The $MgCO_3$ contents in synthetic Ca–Mg carbonates as a function of inactive biomass concentration and initial Mg:Ca ratio in experimental solutions.

Fig. 6. XRD patterns of synthetic Ca–Mg carbonates induced by EPS (27±5 mg/L) of *M. barkeri*. Synthetic calcite (0.2 g/L) was used as seed crystals. Peaks correspond to: A: aragonite; C: calcite seeds; D: Ca-dolomite; H: HMC; M: Monohydrocalcite.

(a): HMC (d_{104} = 3.0186 Å, 5.8 mol% of $MgCO_3$) synthesized in EPS-bearing solutions (Mg:Ca = 3:1). A small amount of aragonite was identified in precipitates.

(b): HMC (d_{104} = 2.9537 Å, 32.1 mol% of $MgCO_3$) synthesized in EPS-bearing solutions (Mg:Ca = 4:1).

(c): Ca-dolomite (d_{104} = 2.9284 Å, 48.0 mol% of $MgCO_3$) synthesized in EPS-bearing solutions (Mg:Ca = 5:1). A small amount of monohydrocalcite was identified in precipitates.

(d): Ca-dolomite (d_{104} = 2.9281 Å, 48.2 mol% of $MgCO_3$) synthesized in EPS-bearing solutions (Mg:Ca = 8:1). A small amount of monohydrocalcite was identified in precipitates.

Fig. 7. Comparison of the catalytic strength of inactive biomass (113±12 mg/L) and EPS (25±7 mg/L). Approximately 25 mg EPS can be extracted from 113 mg biomass following our extraction procedure.

971 **Fig. 8. SEM images of synthetic dolomite. "C" and "D" stand for calcite seed and**
972 **precipitated dolomite, respectively.**
973 **(a):** SEM image of dolomite nano-crystals synthesized in EPS-bearing solutions growing on the
974 surface of a euhedral calcite seed. Arrows indicate precipitated dolomite.
975 **(b):** A close up of the image in **(a)** showing that dolomite occurred as extremely small nano-
976 crystals.
977 **(c):** SEM image showing a calcite seed enclosed by dolomite nano-crystals.
978
979 **Fig. 9. TEM examinations of synthetic dolomite.**
980 **(a):** TEM image of dolomite nano-crystals synthesized in EPS-bearing solutions growing on the
981 surface of a calcite seed. Arrows indicate precipitated dolomite.
982 **(b):** TEM image of dolomite synthesized in EPS-bearing solutions. Dolomite occurred as nano-
983 crystals with a size of ~10-20 nm. Inset is an X-ray EDS spectrum of the synthetic dolomite that
984 contained ~48 mol% of $MgCO_3$.
985 **(c):** SAED pattern of the dolomite in **(b)**. The diffraction arcs suggested that there were low-
986 angle grain boundaries among dolomite nano-crystals. No super-lattice reflections like (003) and
987 $(\bar{1}05)$ were observed on the SAED pattern. Therefore, the synthetic dolomite was disordered.
988 **(d):** High-resolution TEM image from synthetic dolomite. No supper-lattice fringes like (003)
989 and $(\bar{1}05)$ were observed. Inset is a [010] zone axis FFT pattern of the image. No super-lattice
990 reflections were shown on the FFT indicating that the synthetic dolomite was fully disordered.
991
992

Fig. 10. XRD patterns of synthetic Ca–Mg carbonates induced by DCP after EPS extraction. Synthetic calcite (0.2 g/L) was used as seed crystals. Peaks correspond to: A: aragonite; C: calcite seeds; D: Ca-dolomite; H: HMC; M: monohydrocalcite.

(a): Mg-calcite (d_{104} = 3.0301 Å, 2.2 mol% of $MgCO_3$) synthesized in DCP-bearing solutions (87±9 mg/L, Mg:Ca = 3:1). Aragonite was identified in precipitates.

(b): Mg-calcite (d_{104} = 30035 Å, 11.3 mol% of $MgCO_3$) synthesized in DCP-bearing solutions (87±9 mg/L, Mg:Ca = 4:1). Aragonite was identified in precipitates.

(c): Mg-calcite (d_{104} = 2.9980 Å, 13.2 mol% of $MgCO_3$) synthesized in DCP-bearing solutions (87±9 mg/L, Mg:Ca = 5:1). Aragonite was identified in precipitates.

(d): Two phases of Ca–Mg carbonates were precipitated in DCP-bearing solutions (87±9 mg/L, Mg:Ca = 8:1). One is HMC (d_{104} = 2.9657 Å, 25.4 mol% of $MgCO_3$); the other Ca-dolomite (d_{104} = 2.9303 Å, 46.9 mol% of $MgCO_3$). Monohydrocalcite was identified in precipitates.

Table 1 Chemical conditions employed in carbonate precipitation experiments with the non-metabolizing biomass, bound EPS, and DCP and compositions of synthetic carbonates. Errors represent standard deviation.

4

Experiments	Initial Ca^{2+} (mM)	Initial Mg^{2+} (mM)	Initial pH	Final pH	Initial SI_{dd}*	Final Ca^{2+} (mM)	Final Mg^{2+} (mM)	Change in Mg^{2+} (mM)†	Final SI_{dd}*	$MgCO_3$ content based on d_{104} (mol%)‡
Control	5.2±0.2	15.0±0.2	7.8	9.3	5.29	0.05±0.01	14.6±0.2	0.4	3.34	7±1
	5.2±0.2	20.6±0.3	7.8	9.2	5.36	0.09±0.03	20.1±0.3	0.5	3.65	9.1±0.8
	5.2±0.2	24.8±0.1	7.8	9.2	5.39	0.14±0.01	24.2±0.2	0.6	3.87	11.9±0.7
	5.2±0.2	40.5±0.3	7.9	9.2	5.44	0.19±0.01	39.5±0.3	1.0	4.04	18±1
Non-metabolizing Biomass (65±7 mg L^{-1})	5.19±0.08	15.3±0.3	8.1	9.1	-	0.07±0.03	15.0±0.4	0.3	-	5.1±0.6
	5.19±0.08	21.7±0.4	8.2	9.1	-	0.09±0.02	21.0±0.5	0.7	-	12±1.3
	5.19±0.08	26.7±0.7	8.2	9.1	-	0.13±0.03	24.7±0.6	2.0	-	30±1.7
	5.19±0.08	43.0±1.2	8.2	9.2	-	1.05±0.08	40.6±0.6	2.4	-	32±2.1
Non-metabolizing Biomass (113±12 mg L^{-1})	5.1±0.1	15.7±0.3	8.0	9.1	-	0.14±0.04	15.3±0.3	0.4	-	5.7±0.1
	5.1±0.1	20.9±0.4	8.1	9.1	-	0.17±0.04	20.0±0.3	0.9	-	14±1.1
	5.1±0.1	26.5±0.6	8.0	9.0	-	0.20±0.02	23.3±0.5	3.2	-	41±1.3
	5.1±0.1	43.0±1.0	8.1	9.1	-	0.88±0.03	39.9±0.6	3.1	-	45±2.3
Non-metabolizing Biomass (161±17 mg L^{-1})	5.0±0.2	16.0±0.2	7.2	9.0	-	0.14±0.01	14.4±0.3	1.6	-	26±1.1
	5.0±0.2	22.1±0.6	7.4	9.0	-	0.18±0.03	18.1±0.7	4.0	-	42.3±0.3
	5.0±0.2	27.2±0.6	7.5	9.0	-	0.24±0.04	24.5±0.8	2.7	-	48.9±0.6
	5.0±0.2	42.9±0.2	7.5	9.1	-	1.4±0.2	41.1±0.2	1.8	-	-
Bound EPS (25±7 mg L^{-1})	5.0±0.1	15.2±0.5	6.7	9.1	-	0.05±0.01	14.9±0.4	0.3	-	5.4±0.6
	5.0±0.1	20.5±0.4	6.8	9.1	-	0.13±0.01	18.1±0.7	2.4	-	30±2.9
	5.0±0.1	26.1±0.7	7.0	9.0	-	0.16±0.02	22.7±0.7	3.4	-	47±2.1
	5.0±0.1	42.1±0.5	7.1	9.0	-	0.28±0.01	38.1±0.6	4.0	-	48±0.8
DCP (95±9 mg L^{-1})	4.9±0.1	14.8±0.2	6.8	8.9	-	0.23±0.01	14.5±0.4	0.3	-	3.0±1.1
	4.9±0.1	20.4±0.1	6.8	8.9	-	0.12±0.04	19.7±0.4	0.7	-	10±1.6
	4.9±0.1	26.7±0.5	7.1	8.9	-	0.08±0.01	25.9±0.5	0.8	-	15±2
	4.9±0.1	42.4±0.6	7.1	8.9	-	0.06±0.01	39.1±0.3	3.3	-	25±2 and 46±2¶

*Initial and final SI with respect to disordered dolomite. See text for calculation details.
†The difference between initial and final Mg^{2+} concentration.
‡Molar content of $MgCO_3$ in synthetic Ca-Mg carbonates based on the Zhang et al. (2010) curve.
¶Two phases of Ca-Mg carbonate were identified in these precipitates.

Table 2 Analysis of the monosaccharide composition in the polysaccharide fraction of bound EPS.

	mol%
Mannose	36
Ribose	30
Rhamnose	15
Xylose	10
Glucose	7
Fructose	1
Glucuronic acid	1

This is the peer-reviewed, final accepted version for American Mineralogist, published by the Mineralogical Society of America.
The published version is subject to change. Cite as Authors (Year) Title. American Mineralogist, in press.
DOI: https://doi.org/10.2138/am-2020-7381. http://www.minsocam.org/

Figures

Fig. 1. XRD patterns of synthetic Ca–Mg carbonates induced by inactive biomass of *M. barkeri* (113±12 mg/L). Synthetic calcite (0.2 g/L) was used as seed crystals. Peaks correspond to: A: aragonite; C: calcite seeds; D: Ca-dolomite; H: HMC.

(a): HMC (d_{104} = 3.0192 Å, 5.6 mol% of $MgCO_3$) synthesized in inactive biomass-bearing solutions (Mg:Ca = 3:1). A small amount of aragonite was identified in precipitates.

(b): HMC (d_{104} = 2.9926 Å, 15.0 mol% of $MgCO_3$) synthesized in inactive biomass-bearing solutions (Mg:Ca = 4:1). A small amount of aragonite was identified in precipitates.

(c): Ca-dolomite (d_{104} = 2.9388 Å, 41.8 mol% of $MgCO_3$) synthesized in inactive biomass-bearing solutions (Mg:Ca = 5:1).

(d): Ca-dolomite (d_{104} = 2.9305 Å, 46.7 mol% of $MgCO_3$) synthesized in inactive biomass-bearing solutions (Mg:Ca = 8:1).

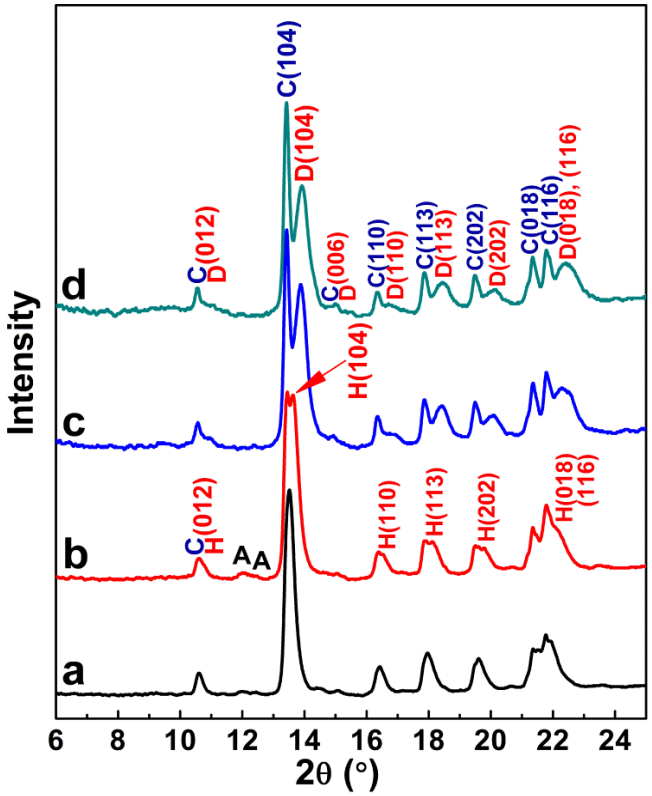

This is the peer-reviewed, final accepted version for American Mineralogist, published by the Mineralogical Society of America.
The published version is subject to change. Cite as Authors (Year) Title. American Mineralogist, in press.
DOI: https://doi.org/10.2138/am-2020-7381. http://www.minsocam.org/

Fig. 2. XRD patterns of synthetic HMC from control experiments with synthetic calcite seeds (0.2 g/L). Peaks correspond to: A: aragonite; C: synthetic calcite; H: HMC.

(a): Aragonite and HMC (d_{104} = 3.0128 Å, 8.4 mol% $MgCO_3$) synthesized in control solutions (Mg:Ca = 3:1).

(b): Aragonite and HMC (d_{104} = 3.0078 Å, 9.5 mol% $MgCO_3$) synthesized in control solutions (Mg:Ca = 4:1).

(c): Aragonite and HMC (d_{104} = 3.0027 Å, 11.5 mol% $MgCO_3$) synthesized in control solutions (Mg:Ca = 5:1).

(d): Aragonite and HMC (d_{104} = 2.9831 Å, 18.5 mol% $MgCO_3$) synthesized in control solutions (Mg:Ca = 8:1).

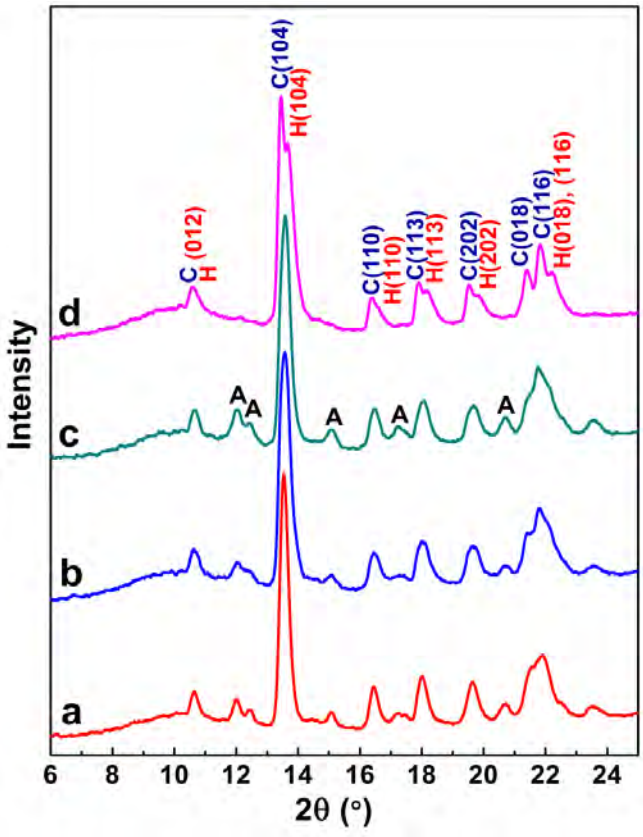

This is the peer-reviewed, final accepted version for American Mineralogist, published by the Mineralogical Society of America.
The published version is subject to change. Cite as Authors (Year) Title. American Mineralogist, in press.
DOI: https://doi.org/10.2138/am-2020-7381. http://www.minsocam.org/

Fig. 3. XRD patterns of synthetic Ca–Mg carbonates induced by inactive biomass of *M. barkeri* (65±7 mg/L). Synthetic calcite (0.2 g/L) was used as seed crystals. Peaks correspond to: A: aragonite; C: calcite seeds; H: HMC.

(a): HMC (d_{104} = 3.0215 Å, 4.7 mol% of $MgCO_3$) synthesized in inactive biomass-bearing solutions (Mg:Ca = 3:1). A small amount of aragonite was identified in precipitates.

(b): HMC (d_{104} = 3.0004 Å, 12.5 mol% of $MgCO_3$) synthesized in inactive biomass-bearing solutions (Mg:Ca = 4:1). A small amount of aragonite was identified in precipitates.

(c): HMC (d_{104} = 2.9590 Å, 28.6 mol% of $MgCO_3$) synthesized in inactive biomass-bearing solutions (Mg:Ca = 5:1).

(d): HMC (d_{104} = 2.9568 Å, 30.0 mol% of $MgCO_3$) synthesized in inactive biomass-bearing solutions (Mg:Ca = 8:1).

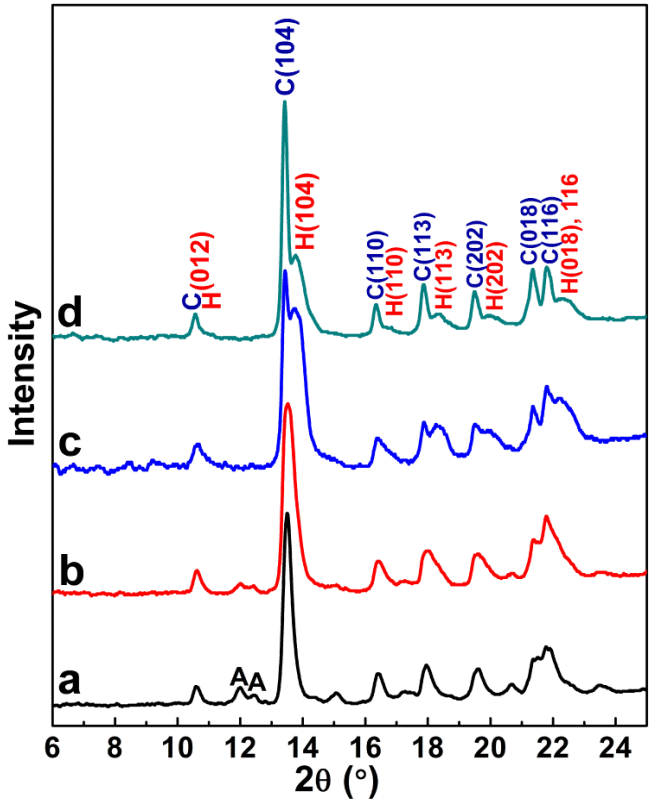

This is the peer-reviewed, final accepted version for American Mineralogist, published by the Mineralogical Society of America.
The published version is subject to change. Cite as Authors (Year) Title. American Mineralogist, in press.
DOI: https://doi.org/10.2138/am-2020-7381. http://www.minsocam.org/

Fig. 4. XRD patterns of synthetic Ca–Mg carbonates induced by inactive biomass of *M. barkeri* (161±17 mg/L). Synthetic calcite (0.2 g/L) was used as seed crystals. Peaks correspond to: A: aragonite; C: calcite seeds; D: Ca-dolomite; H: HMC; M: monohydrocalcite.

(a): HMC (d_{104} = 2.9611 Å, 26.7 mol% of $MgCO_3$) synthesized in inactive biomass-bearing solutions (Mg:Ca = 3:1). A small amount of monohydrocalcite was observed in precipitates.

(b): Ca-dolomite (d_{104} = 2.9373 Å, 42.7 mol% of $MgCO_3$) synthesized in inactive biomass-bearing solutions (Mg:Ca = 4:1). Monohydrocalcite was identified in precipitates.

(c): Ca-dolomite (d_{104} = 2.9256 Å, 49.3 mol% of $MgCO_3$) synthesized in inactive biomass-bearing solutions (Mg:Ca = 5:1). Monohydrocalcite was identified in precipitates.

(d): No crystalline Ca–Mg carbonate precipitation was observed in inactive biomass-bearing solutions (Mg:Ca = 8:1). Monohydrocalcite was identified in precipitates.

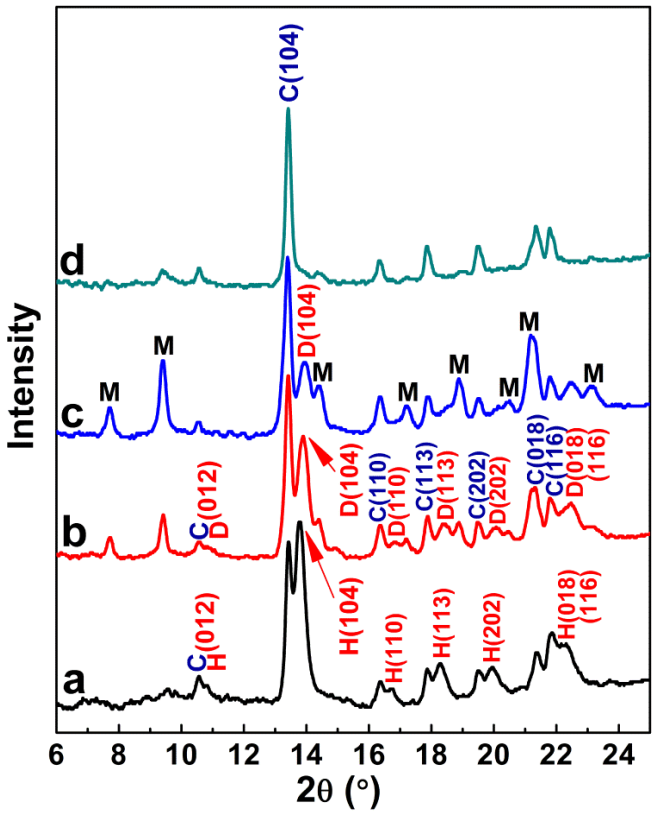

Fig. 5. The $MgCO_3$ contents in synthetic Ca–Mg carbonates as a function of inactive biomass concentration and initial Mg:Ca ratio in experimental solutions.

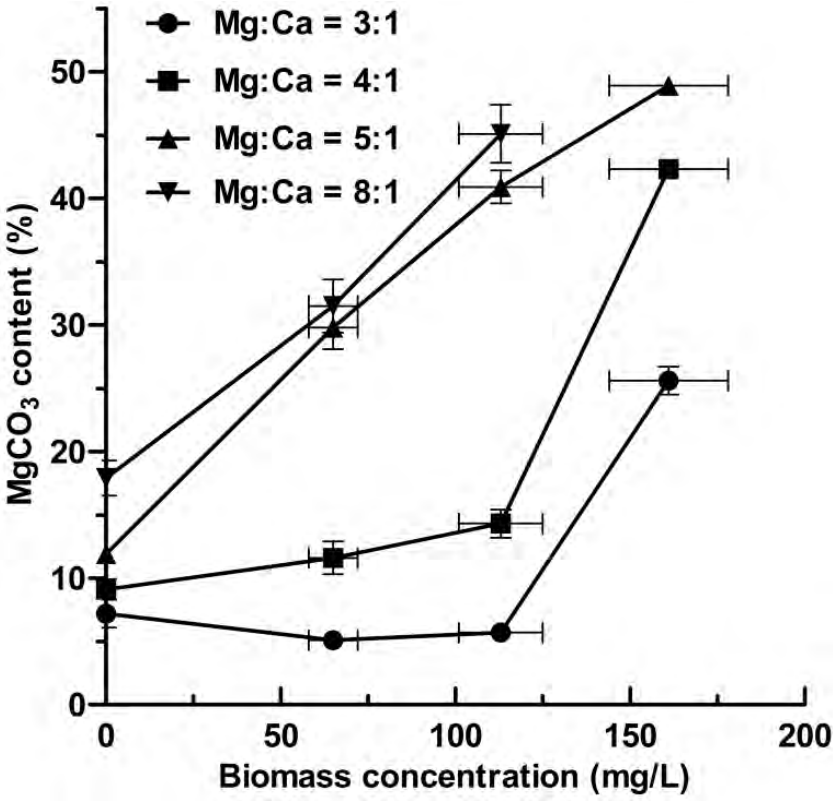

This is the peer-reviewed, final accepted version for American Mineralogist, published by the Mineralogical Society of America.
The published version is subject to change. Cite as Authors (Year) Title. American Mineralogist, in press.
DOI: https://doi.org/10.2138/am-2020-7381. http://www.minsocam.org/

Fig. 6. XRD patterns of synthetic Ca–Mg carbonates induced by EPS (27±5 mg/L) of *M. barkeri*. Synthetic calcite (0.2 g/L) was used as seed crystals. Peaks correspond to: A: aragonite; C: calcite seeds; D: Ca-dolomite; H: HMC; M: Monohydrocalcite.

(a): HMC (d_{104} = 3.0186 Å, 5.8 mol% of $MgCO_3$) synthesized in EPS-bearing solutions (Mg:Ca = 3:1). A small amount of aragonite was identified in precipitates.

(b): HMC (d_{104} = 2.9537 Å, 32.1 mol% of $MgCO_3$) synthesized in EPS-bearing solutions (Mg:Ca = 4:1).

(c): Ca-dolomite (d_{104} = 2.9284 Å, 48.0 mol% of $MgCO_3$) synthesized in EPS-bearing solutions (Mg:Ca = 5:1). A small amount of monohydrocalcite was identified in precipitates.

(d): Ca-dolomite (d_{104} = 2.9281 Å, 48.2 mol% of $MgCO_3$) synthesized in EPS-bearing solutions (Mg:Ca = 8:1). A small amount of monohydrocalcite was identified in precipitates.

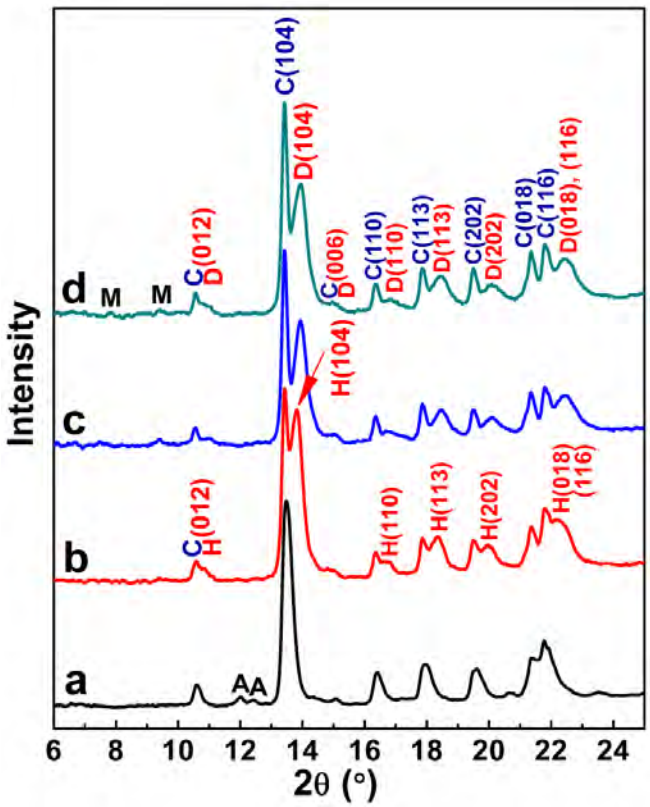

Fig. 7. Comparison of the catalytic strength of inactive biomass (113±12 mg/L) and EPS (25±7 mg/L). Approximately 25 mg EPS can be extracted from 113 mg biomass following our extraction procedure.

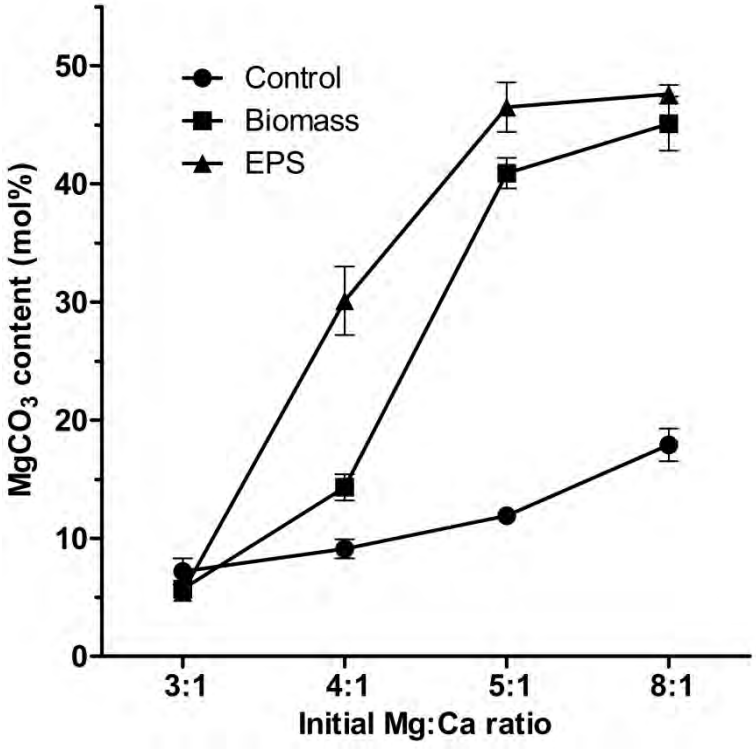

This is the peer-reviewed, final accepted version for American Mineralogist, published by the Mineralogical Society of America.
The published version is subject to change. Cite as Authors (Year) Title. American Mineralogist, in press.
DOI: https://doi.org/10.2138/am-2020-7381. http://www.minsocam.org/

Fig. 8. SEM images of synthetic dolomite. "C" and "D" stand for calcite seed and precipitated dolomite, respectively.

(a): SEM image of dolomite nano-crystals synthesized in EPS-bearing solutions growing on the surface of a euhedral calcite seed. Arrows indicate precipitated dolomite.

(b): A close up of the image in **(a)** showing that dolomite occurred as extremely small nano-crystals.

(c): SEM image showing a calcite seed enclosed by dolomite nano-crystals.

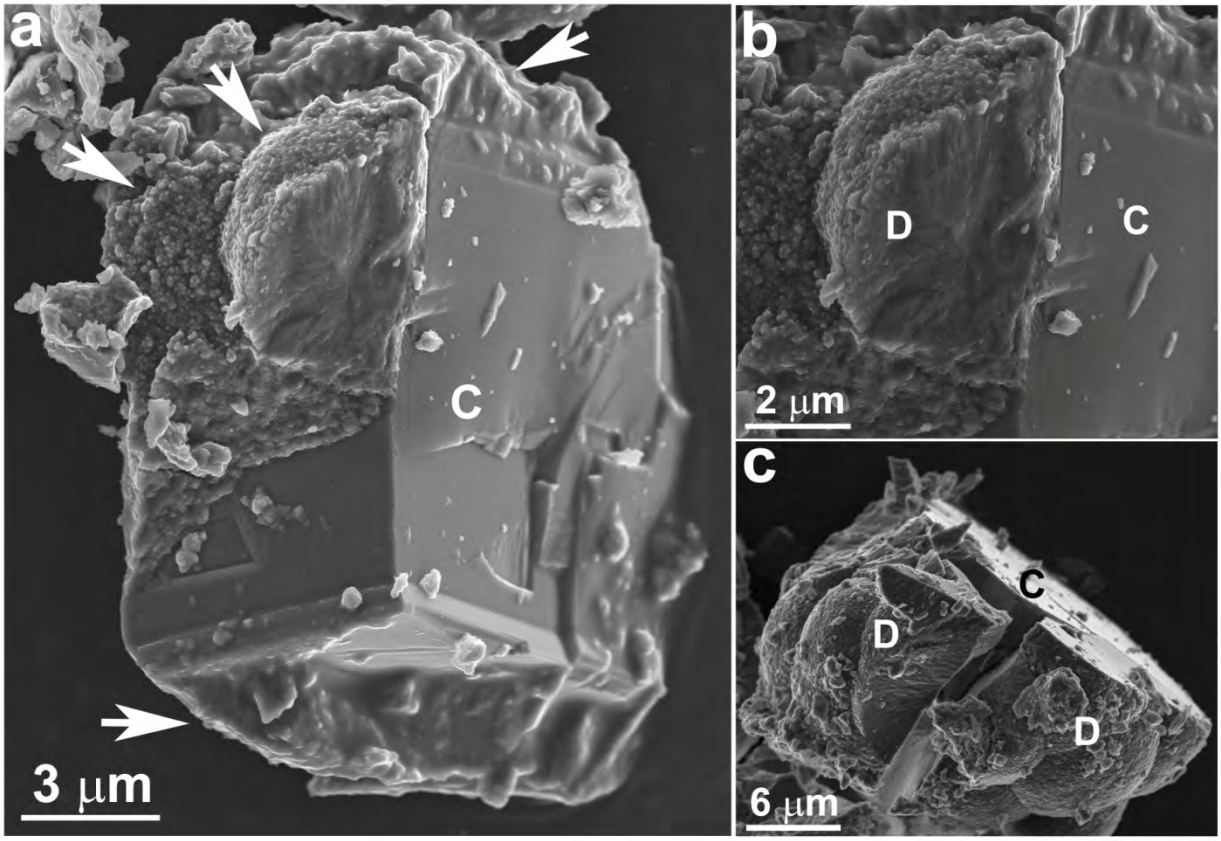

This is the peer-reviewed, final accepted version for American Mineralogist, published by the Mineralogical Society of America.
The published version is subject to change. Cite as Authors (Year) Title. American Mineralogist, in press.
DOI: https://doi.org/10.2138/am-2020-7381. http://www.minsocam.org/

Fig. 9. TEM examinations of synthetic dolomite.

(a): TEM image of dolomite nano-crystals synthesized in EPS-bearing solutions growing on the surface of a calcite seed. Arrows indicate precipitated dolomite.

(b): TEM image of dolomite synthesized in EPS-bearing solutions. Dolomite occurred as nano-crystals with a size of ~10-20 nm. Inset is an X-ray EDS spectrum of the synthetic dolomite that contained ~48 mol% of $MgCO_3$.

(c): SAED pattern of the dolomite in **(b)**. The diffraction arcs suggested that there were low-angle grain boundaries among dolomite nano-crystals. No super-lattice reflections like (003) and ($\bar{1}$05) were observed on the SAED pattern. Therefore, the synthetic dolomite was disordered.

(d): High-resolution TEM image from synthetic dolomite. No supper-lattice fringes like (003) and ($\bar{1}$05) were observed. Inset is a [010] zone axis FFT pattern of the image. No super-lattice reflections were shown on the FFT indicating that the synthetic dolomite was fully disordered.

This is the peer-reviewed, final accepted version for American Mineralogist, published by the Mineralogical Society of America.
The published version is subject to change. Cite as Authors (Year) Title. American Mineralogist, in press.
DOI: https://doi.org/10.2138/am-2020-7381. http://www.minsocam.org/

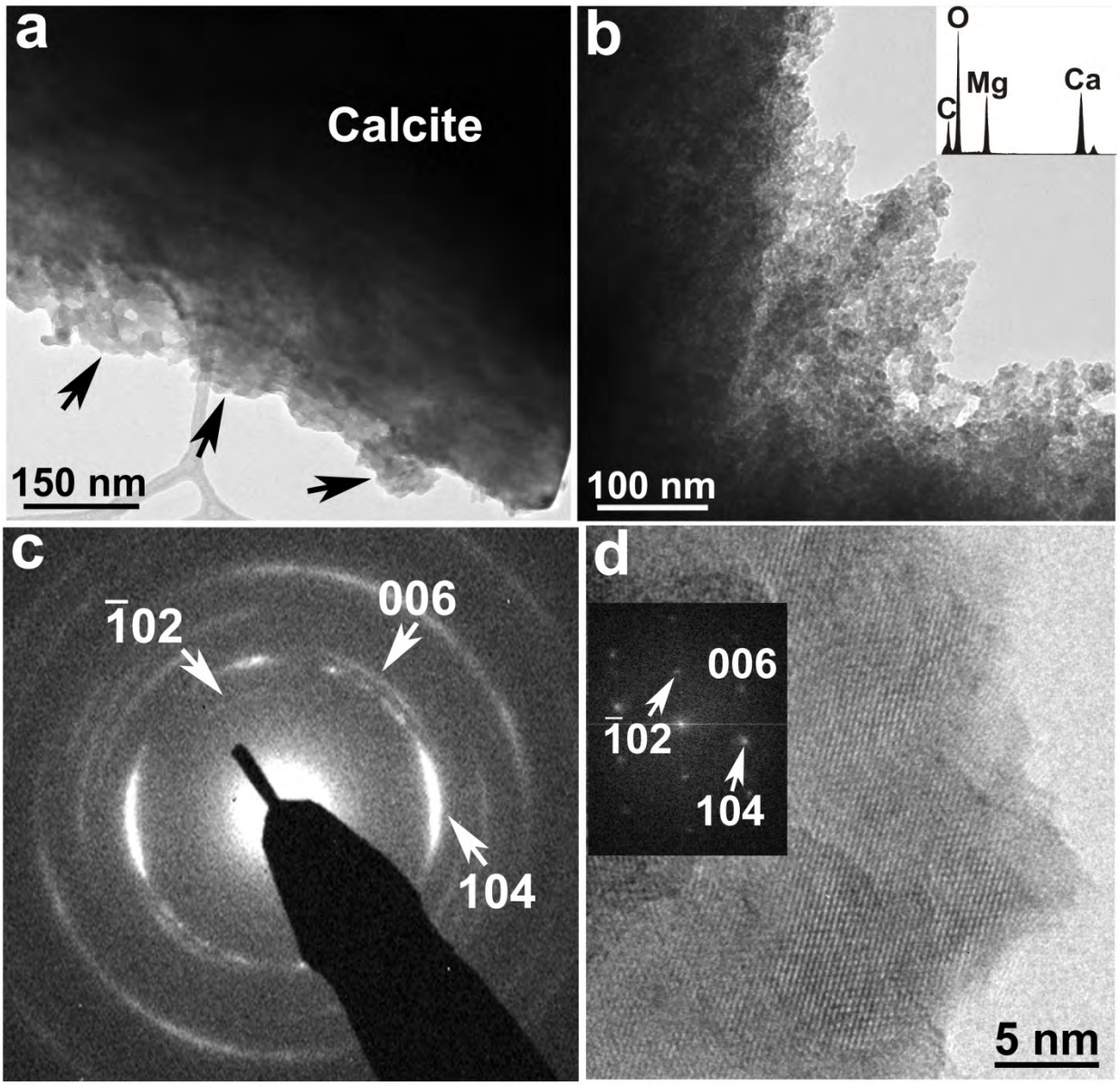

This is the peer-reviewed, final accepted version for American Mineralogist, published by the Mineralogical Society of America.
The published version is subject to change. Cite as Authors (Year) Title. American Mineralogist, in press.
DOI: https://doi.org/10.2138/am-2020-7381. http://www.minsocam.org/

Fig. 10. XRD patterns of synthetic Ca–Mg carbonates induced by DCP after EPS extraction. Synthetic calcite (0.2 g/L) was used as seed crystals. Peaks correspond to: A: aragonite; C: calcite seeds; D: Ca-dolomite; H: HMC; M: monohydrocalcite.

(a): Mg-calcite (d_{104} = 3.0301 Å, 2.2 mol% of $MgCO_3$) synthesized in DCP-bearing solutions (87±9 mg/L, Mg:Ca = 3:1). Aragonite was identified in precipitates.

(b): Mg-calcite (d_{104} = 30035 Å, 11.3 mol% of $MgCO_3$) synthesized in DCP-bearing solutions (87±9 mg/L, Mg:Ca = 4:1). Aragonite was identified in precipitates.

(c): Mg-calcite (d_{104} = 2.9980 Å, 13.2 mol% of $MgCO_3$) synthesized in DCP-bearing solutions (87±9 mg/L, Mg:Ca = 5:1). Aragonite was identified in precipitates.

(d): Two phases of Ca–Mg carbonates were precipitated in DCP-bearing solutions (87±9 mg/L, Mg:Ca = 8:1). One is HMC (d_{104} = 2.9657 Å, 25.4 mol% of $MgCO_3$); the other Ca-dolomite (d_{104} = 2.9303 Å, 46.9 mol% of $MgCO_3$). Monohydrocalcite was identified in precipitates.